August 2023

Multi-Order Modeling of Linear Magnetic Motor System

Ming-Jen Chen
University of Wisconsin-Milwaukee

MULTI-ORDER MODELING OF LINEAR MAGNETIC MOTOR SYSTEM

by

MING-JEN CHEN

A Thesis Submitted in

Partial Fulfillment of the

Requirements for the Degree of

Master of Science

in Engineering

at

The University of Wisconsin-Milwaukee

August 2023

ABSTRACT

MULTI-ORDER MODELING OF LINEAR MAGNETIC MOTOR SYSTEM

by

MING-JEN CHEN

The University of Wisconsin-Milwaukee, 2023
Under the Supervision of Professor Ilya Avdeev

Numerical simulations have been proven to be a powerful tool for predicting, testing, and validating the capabilities of new designs. However, given the high demand for simulating extremely complicated geometries and nonlinear physical phenomena, simulations can often be significantly time consuming. Consequently, the development of high-precision reduced-order models becomes indispensable to reduce computational time. In this study, we simplified and characterized an industrial motion system based on linear magnetic motor technology using accurate full 3-D numerical model. The system behavior was explored through various scenarios, including extreme conditions, to gain a deeper understanding of its thermal behavior during operation. The simulation results were then compared with experimental measurements. To achieve model order reduction, the initial and boundary conditions, along with temperature distributions derived from the simulation results, were translated into excitations and outputs for constructing robust reduced-order models. Subsequently, the reduced order model was thoroughly tested and validated against new scenarios derived from the 3-D simulation results.

Dedicated to the steadfast support of my family, friends, and faculty mentors.
A special and profound thank you to my Mother, Feng-Min Liu, whose words have been my guiding light throughout my studies.

TABLE OF CONTENTS

LIST OF FIGURES vi

LIST OF TABLES viii

ACKNOWLEDGEMENTS ix

1. Introduction 1

2. Literature Review 5

2.1 Physical Model 7

2.2 Mathematical model 11

2.3 3-D Numerical Model 12

2.4 Reduced-Order Modeling 19

2.5 Experimental Setup for Data Acquisitions 23

3. Results 25

3.1 Numerical Convergence Test 25

3.2 3-D Simulation Results 28

3.3 Reduced-Order Modeling Results 35

3.4 Experimental Results 39

4. Summary of Results 41

4.1 Mesh Convergence Test 41

4.2 Transient 3-D Simulation and Thermal Experiment 42

4.3 Reduced-order model building and validating 44

4.4 Comparing Time: Full 3-D vs. Dynamic ROM Simulations 44

5. Future Work 46

References 47

LIST OF FIGURES

Figure 1.1 Materials Distributed Along the Manufacturing line [28] 2

Figure 1.2 Different Configurations of Linear Magnetic Motors 4

Figure 2.1 250-mm Linear Magnetic Motor Drawing 8

Figure 2.2 Puck Drawing (Moving Magnetic Part) 9

Figure 2.3 Halbach Array 9

Figure 2.4 Full assembly of a 250-mm linear magnetic motor 10

Figure 2.5 Full Physical Model of the Linear Magnetic Motors (Entire System) 13

Figure 2.6 Full 3-D CAD Model of Linear Magnetic Motor (One Motor) 13

Figure 2.7 Simplified CAD Model 15

Figure 2.8 Tetrahedral Mesh of EPDM Rubber 16

Figure 2.9 Tetrahedral and Hexahedral Elements Mesh of Coils 17

Figure 2.10 The Workflow of Building a Dynamic Reduced-Order Model 20

Figure 2.11 Single-Layer Neural Network 21

Figure 2.12 The Schematics of Data Acquisition Process 24

Figure 2.13 The Experimental Setup: Temperature Sensors' Placement 24

Figure 3.1 Maximum Temperatures Between Four Difference Mesh Sizes 26

Figure 3.2 The Difference of Four Meshes 27

Figure 3.3 Undershooting of 10mm Meshes 27

Figure 3.4 Undershooting of 7.5mm Meshes 27

Figure 3.5 The Temperature Distribution on Coils with 10W Load 29

Figure 3.6 The Temperature Tistribution on Wrap (EPDM Rubber) with 10W Load 29

Figure 3.7 The Temperature Distribution on Coils with 15W Load 30

Figure 3.8 The Temperature Distribution on Wrap (EPDM Rubber) with 15W Load 30

Figure 3.9 The Temperature Distribution on Coils with 20W Load 31

Figure 3.10 The Temperature Distribution on Wrap (EPDM Rubber) with 20W Load 31

Figure 3.11 The Temperature Distribution on Coils with 25W Load 32

Figure 3.12 The Temperature Distribution on Wrap (EPDM Rubber) with 25W Load 32

Figure 3.13 The Temperature Distribution on Coils with 30W Load 33

Figure 3.14 The Temperature Distribution on Wrap (EPDM Rubber) with 30W Load33

Figure 3.15 The Temperature Distribution on Coils with 35W Load 34

Figure 3.16 The Temperature Distribution on Wrap (EPDM Rubber) with 35W Load 34

Figure 3.17 The Result from 3-D Simulation.....36

Figure 3.18 The Result of 3-D Simulations and ROMs 36

Figure 3.19 The Errors between 3-D Simulations and ROMs 37

Figure 3.20 The Testing Result of ROM with 23W Load.....38

Figure 3.21 The Validating Result of 3-D Simulation with 23W Load 38

Figure 3.22 Result of ROM vs. Result of 3-D Simulation 39

Figure 3.23 Temperature Monitoring at the Surface of the Motor.....40

Figure 4.1 Temperature Monitoring at the Surface of the Motor.....43

Figure 4.2 Transient Thermal Simulation Result with 20W Load 43

Figure 4.3 Time Consumption for 6,000 sec Transient Simulation 45

LIST OF TABLES

Table 2-1 The Limitations of the Linear Magnetic Motor 10

Table 2-2 Material Properties of EPDM Rubber 17

Table 2-3 Material Properties of the Coil 18

Table 2-4 Initial Conditions and Boundary Conditions 19

Table 4-1 Time Consumption of for 6000 sec transient simulation 45

ACKNOWLEDGEMENTS

Completing my master's degree was no easy task, and I couldn't have done it without the help and support. A big thank you to Dr. Ilya Avdeev, my thesis advisor. His advice and insights were always spot-on, helping me both in my studies and in making career decisions. I extend my heartfelt thanks to my defense committee: Dr. Woo-Jin Chang and Dr. Konstantin Sobolev. Your expertise and guidance have been indispensable.

I'm also really grateful to my labmate, Manuel Garmendez. He was always there to remind me to take a step back and not get too lost in the details. Edgar Garza also played a big role, always pushing me to take care of my health and stay active. It made a huge difference.

Many others have helped me along the way too. To all of you, I want to say a sincere "thank you."Putting my gratitude into words isn't always easy, but I hope everyone knows how much I appreciate their support.

1. Introduction

Manufacturing industries, such as microelectronics, metal manufacturing and food processing are established with a focus on mass production. Generally, three distinct manufacturing production models have been adopted by these and other industries: make-to-stock, make-to-order, and make-to-assembly.

Make-to-stock (MTS) represents a manufacturing production model in which products and goods are manufactured prior to receiving orders. In this approach, manufacturing companies may assume the risk of producing an excess of parts, components, goods or merchandise. However, it proves to be an optimal strategy for suppliers of products with consistent demand, such as construction parts, auto components, as it enables swift order fulfillment.

Make-to-order (MTO) stands in stark contrast to the MTS model. With MTO, manufacturing companies initiate the production of parts only upon receiving orders from their customers. This approach alleviates the need for manufacturing companies to shoulder the burden of excessive product inventory in their warehouses. Nevertheless, it introduces concerns about meeting demand promptly and the potential for competitors to seize the remaining portion of the order.

Make-to-assembly (MTA) can be seen as a hybrid production model that combines elements of both MTS and MTO. In this approach, manufacturing companies pre-produce the core parts and components required for the final product, but the assembly of the ultimate product is deferred until customer orders are received.

All manufacturing models rely on transportation systems to facilitate the movement of materials, parts, components or final goods between different stations of the production line.

Factories use these transportation systems to ensure the accurate and efficient conveyance of materials and discrete parts [1]. This process is illustrated in Figure 1.1, where the manufacturing materials are observed to be distributed along the manufacturing production line at any given point of time.

Figure 1.1 Materials Distributed Along the Manufacturing line [28]

A reliable transportation system is essential for both production lines and assembly lines to effectively satisfy the demands of mass production. Historically, conveyor systems have been the predominant technology harnessed within manufacturing. A foundational conveyor system typically comprises components such as rollers, belts or chains, and motors. These conveyors convert the rotational motion of the motor into linear motion facilitating the movement of part within the factory.

Broadly, three distinct conveyor types exist: chain belt conveyors, slider bed conveyors, and steel belt conveyors. These variants offer several noteworthy advantages, including time savings, easy controllability, and reduced reliance on human effort. Despite the numerous benefits associated with these conveyor systems, the cost of maintenance emerges as a notable concern for manufacturing facilities. Most factories that use conveyor as their

transporting system maintain an ample stock of spare parts to mitigate the impact of unexpected downtime, which is considered to be a serious concern with significant economic impact on the overall business.

In addition to conventional conveyor systems, linear electric motors serve as viable alternative. Analogous to the rotational electric motors, linear motors consist of two parts: a rotor and a stator. The rotor encompasses coils, while the stator features a magnetic array. In a rotational motor, the application of current to the coils induces rotational motion. In contrast, a linear motor could be seen as an extension of a rotational motor, generating linear movement and force.

Linear motors could be categorized into seven different types: Brush, Brushless, Induction Homopolar, Tubular, Piezo Electric and Synchronous. In this research, we are going to focus on linear magnetic motor technology. As mentioned earlier, linear magnetic motors follow the same physical principles as their rotational counterparts. Nonetheless, their design offers increased versatility for integration into production lines. Notably, the modular structure of linear magnetic motors enables the connection of multiple motors based on the design need, as depicted in Figure 1.2 [4].

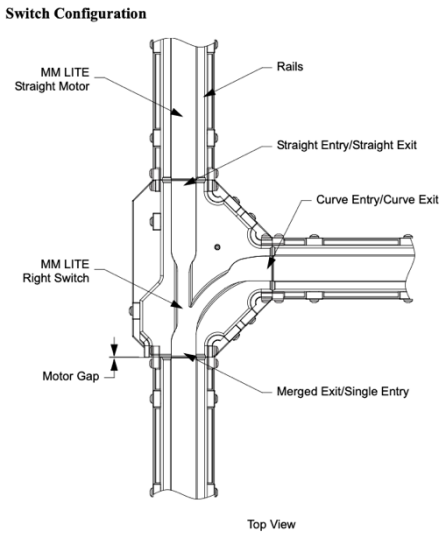

(a) Switch Configuration

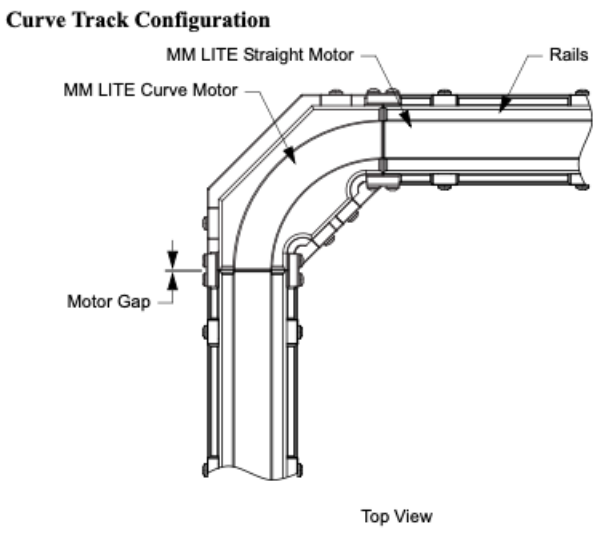

(b) Curve Track Configuration

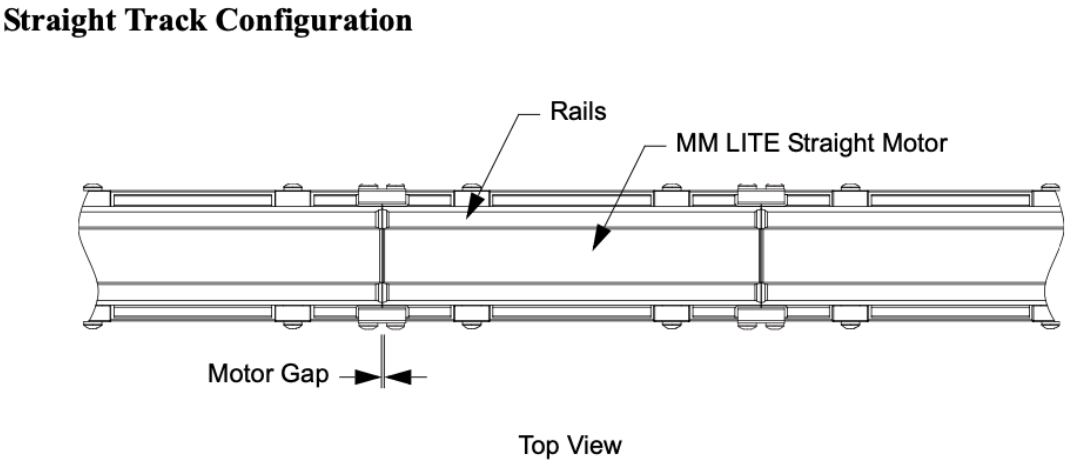

(C) Straight Track Configuration

Figure 1.2 Different Configurations of Linear Magnetic Motors

In this scenario, production lines can effectively optimize traffic flow to achieve maximum throughput through the application of Operation Research principles. Furthermore, individual motor operation enables bidirectional propulsion and variable pitch adjustment, catering to diverse vehicles requirements. Adding to their advantages, linear magnetic motors boast simple designs reducing the overall cost of maintenance [3].

Nonetheless, heat generation and dissipation require thorough consideration when employing linear magnetic motors in production [5]. This concern imposes constraints on design of the manufacturing transporting systems. Various systems may incorporate active cooling or passive cooling mechanisms, each presenting distinct advantages and disadvantages [6], [7]. Modern production lines are frequently conceptualized and executed in collaboration with Original Equipment Manufacturers (OEMs), as exemplified by Rockwell Automation's *MagneMotion* system.

Designing and assembling a linear magnetic system with heat considerations in mind requires comprehensive understanding of the production loads and schedule and environmental variables, such as ambient temperature, humidity etc. Modeling and predicting large-scale system electromagnetic-thermal behavior is essential for design of such systems. This work contributes to the body of knowledge related to system modeling by probing model order reduction approach to capturing dynamic thermal behavior of a real linear magnetic system.

2. Literature Review

The remarkable advancements in semiconductor technology have led to a notably accelerated enhancement in engineering computing. These developments outpaced the evolution of manufacturing engineering systems themselves. It becomes more feasible to simulate an entire production system in order to design and produce it. Typically, finite element analysis (FEA) models are deployed to that end. However, an emerging demand has arisen to replicate these intricate systems in real-time or to forecast potential failures arising from shifting environmental or load conditions. Yet, the conventional approach that involves full 3-D FEA models proves too complicated for most manufacturing end-users or OEMs

designing and integrating such systems. A model order reduction can offer model flexibility and design speed that makes system-level design for heat failure prevention attainable.

The initial application of model order reduction dates to 1967 when it was employed to address the challenges posed by inhomogeneous turbulent flows [8]. Since then, the model order reduction has been used broadly for simplifying problem-complexity and to reduce the compute time.

In the realm of model order reduction for thermal management of electromagnetic motors, significant research efforts have been directed towards eccentricity [9], thermal distribution [10], and optimization [11]. Most of these concerns manifest within rotational magnetic motors. However, due to the inherent structural differences between rotational and linear motors, understanding of the linear motor's behavior is essential.

The unique structure of linear magnetic motors enables the seamless connection of multiple units, facilitating development of complex transportation systems. This distinctive feature empowers linear magnetic motors to pave the way for long-distance and high-speed transportation systems. One prominent example is the magnetic levitation (maglev) train, a popular mode of commuting and travel. In this context, Japan's pursuit of an economical and swifter maglev system exemplifies the ongoing efforts in this field [13].

However, the development of such an intricate system cannot rely solely on trial and error, given its potential cost implications. Employing finite element analysis offers a more reasoned and viable approach for crafting this ambitious system. Yet, the maglev system presents a substantial-scale model for finite element method applications, necessitating extensive simulation times. Consequently, the prevalent trajectory in finite element analysis involves the construction of reduced-order models to expedite simulations, as exemplified in recent research trends [14], [15], [16], [17], [18].

Another significant application of linear magnetic motors lies in the transportation systems within manufacturing factories – the focus of this research. As previously discussed, the establishment of an efficient transportation infrastructure for production lines is imperative for achieving mass production targets across various manufacturing entities. Depending on the specific requirements and contextual environmental factors, Original Equipment Manufacturers (OEMs) must be equipped to provide tailored solutions to their clientele. Nonetheless, much of the existing research in this domain has predominantly focused on the performance and thermal characteristics of linear actuators, often employing model order reduction techniques [19], [20]. While these approaches undeniably contribute to understanding of the key principles and thermal dynamics of linear actuators, there remains an unexplored space of multi-order modeling of linear magnetic motors within the manufacturing application space.

2.1 Physical Model

The physical real-world system under investigation encompasses a magnetic configuration comprising both mobile and stationary components. The moving part, referred to as a "puck," is composed of five permanent magnets. To optimize the magnetic flux on one side and thereby enhance performance, these magnets are arranged in a Halbach Array configuration [22]. The stationary component, on the other hand, constitutes the motor, characterized by coreless coils. This strategic design choice, notably the absence of a steel core, effectively mitigates the cogging effect associated with such linear magnetic motor systems [23], [24]. For a visual representation, the mechanical blueprints and structural attributes of both the puck and the motor are illustrated in Figure 2.1, Figure 2.2, Figure 2.3, and Figure 2.4.

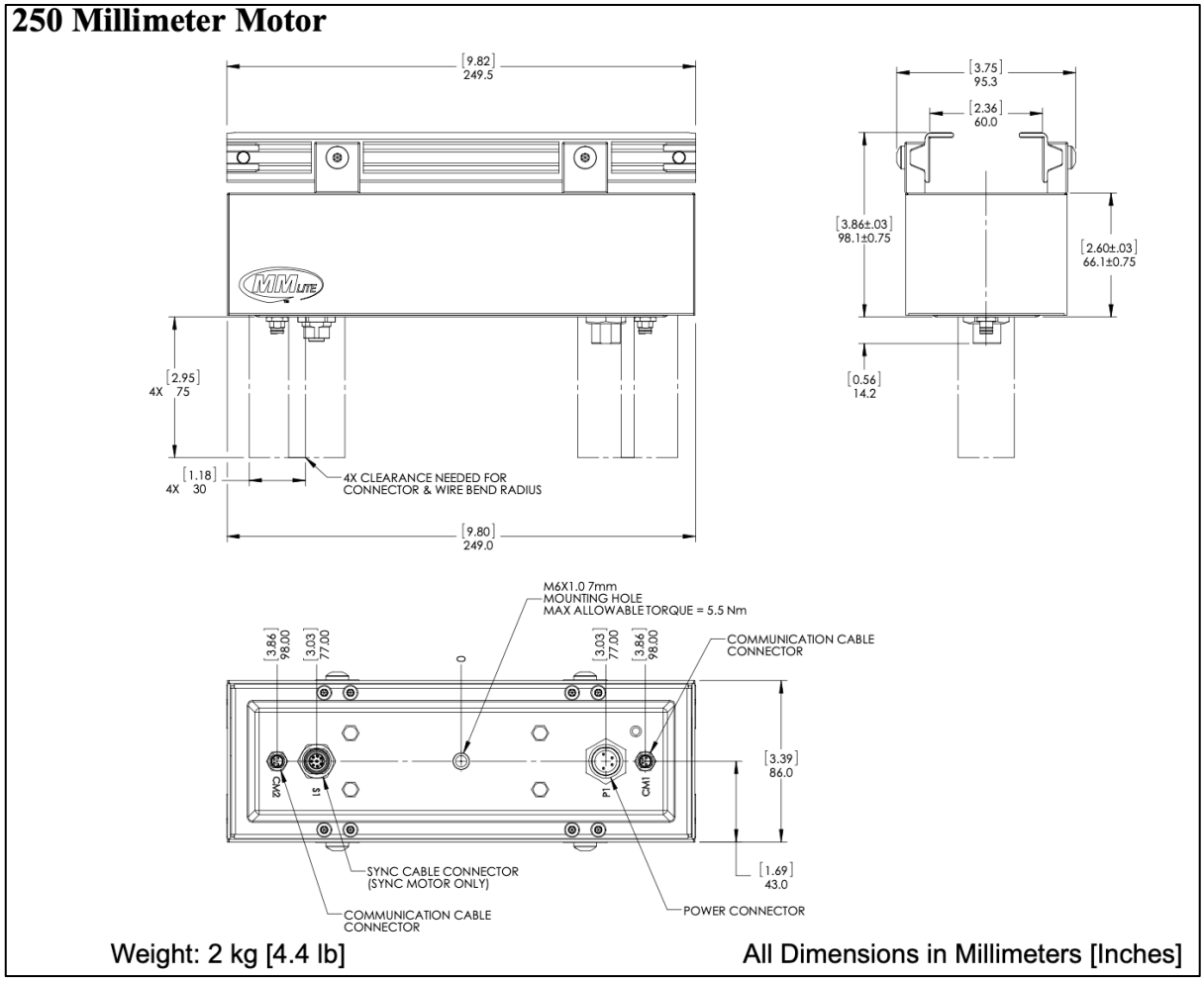

Figure 2.1 250-mm Linear Magnetic Motor Drawing

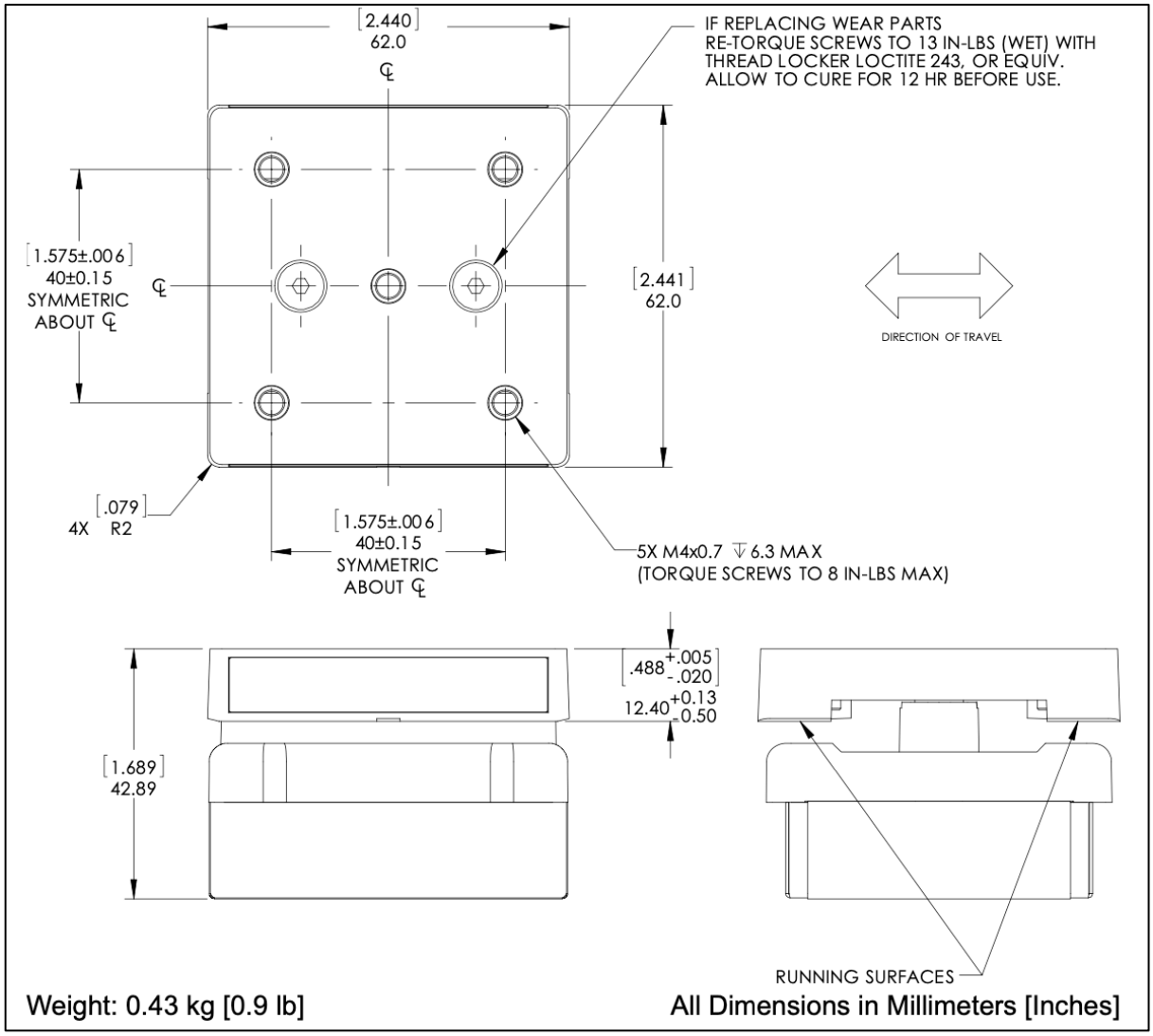

Figure 2.2 Puck Drawing (Moving Magnetic Part)

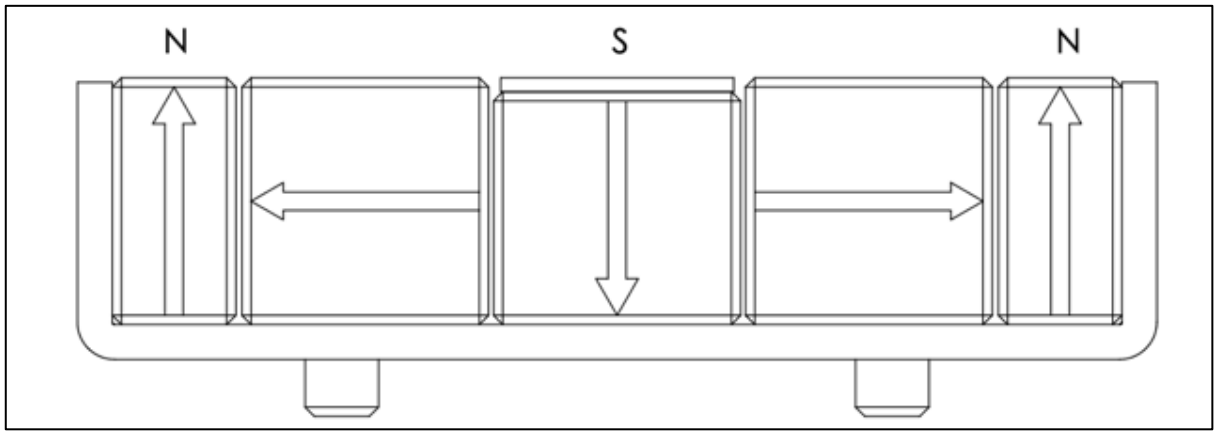

Figure 2.3 Halbach Array

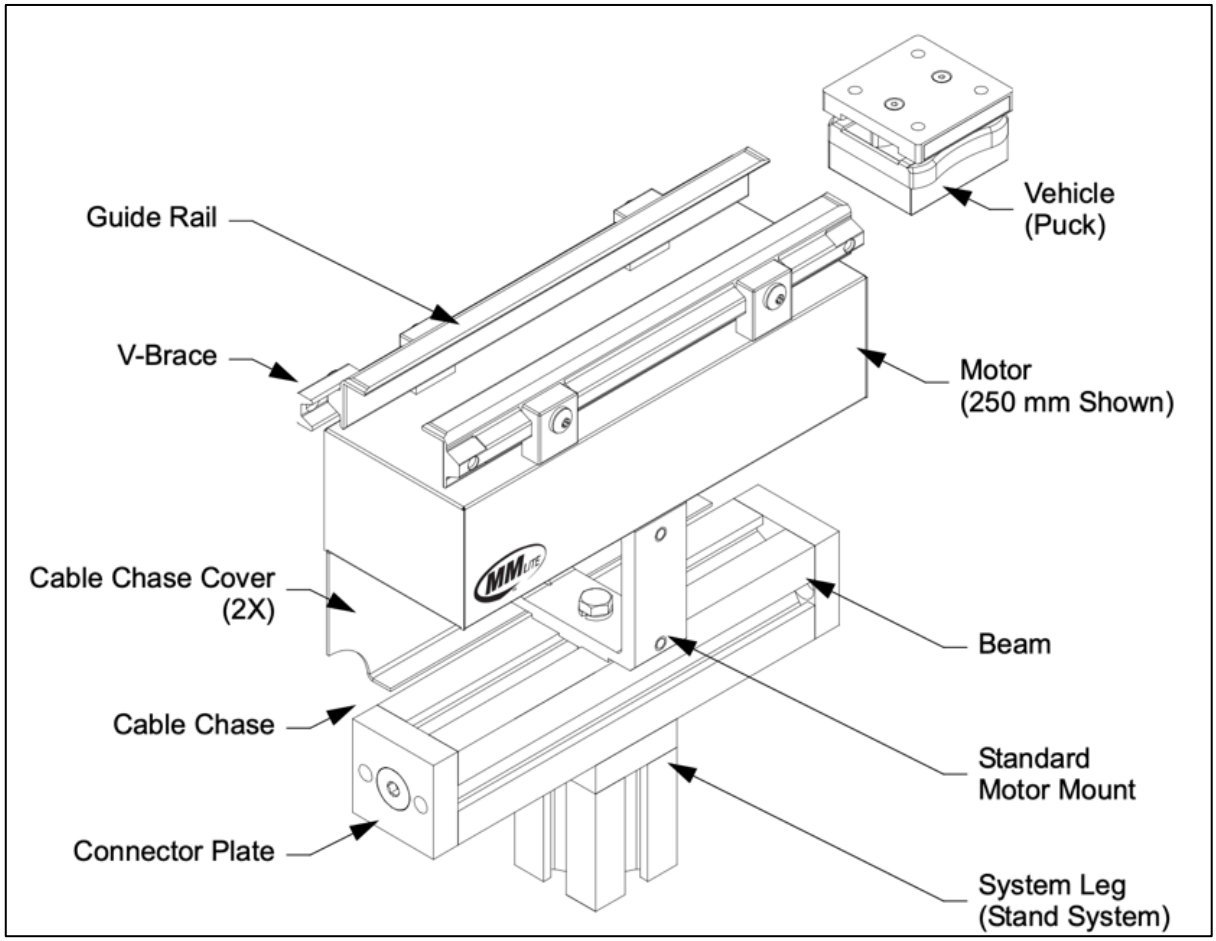

Figure 2.4 Full assembly of a 250-mm linear magnetic motor

The performance parameters of the linear magnetic motor are shown in Table 2-1.

Table 2-1 The Limitations of the Linear Magnetic Motor

Maximum Velocity	2.0 m/s
Maximum Acceleration	9.0 m/s^2
Thrust	6.0 N/cycle
Maximum Payload	2.0 kg
Maximum Power	35 W

2.2 Mathematical model

In this study, our focus centers on comprehending the thermal dynamics inherent to the linear magnet driving system. The heat transfer mechanisms governing the behavior of the system are encapsulated by the following equation:

$$\Delta H = m \times s \times \Delta \mathrm{T} \tag{2.1}$$

Where ΔH is the heat supplied to the system, m is the mass, s is the specific heat capacity and $\Delta \mathrm{T}$ is the temperature change.

Generally speaking, three primary modes of heat transfer present in the electromechanical motor systems: conduction, convection, and radiation. However, within the scope of this study, our focus is directed solely towards the coil and rubber components housed within the metal cover. Recognizing that metal exhibits substantial insulating properties concerning heat transfer via radiation [29], we opt to disregard the radiation term within this mathematical model. As a consequence, our mathematical representation predominantly encapsulates the thermal conduction and thermal convection aspects, as illustrated by the equations provided below (Eq. 2.2 and 2.3).

For thermal conduction:

$$Q = \frac{kA(T_{Hot} - T_{Cold})_t}{d} \tag{2.2}$$

Where:

Q: The Rate of heat transfer

k : The coefficient of thermal conductivity

A : The contact area.

T : The temperature

t : Time

d : Thickness of the material

For thermal convection, the governing equation is:

$$Q = H_c A(T_{Hot} - T_{Cold}) \tag{2.3}$$

Where:

H_c : Heat Transfer Coefficient of the material

2.3 3-D Numerical Model

Our approach involves addressing heat transfer via the Finite Element Method. The computational model is formulated based on certain underlying assumptions, which we outline below. Our current investigation is focused on constructing models of varying orders and delving into the analysis of Joule heat within the linear magnet driving system. We treat this scenario as a transient thermal problem, wherein the coils of the linear motor continuously generate heat. Our computational framework necessitates considering key parameters, such as thermal conductivity, film coefficient, and room temperature, which serve as vital boundary conditions for computing the temperature distribution across the linear magnetic motor.

To build the robust FEA numerical model, we must simplify system's physical representation. The visual depiction of both the physical and 3-D models is encapsulated in Figure 2.5 and Figure 2.6, respectively.

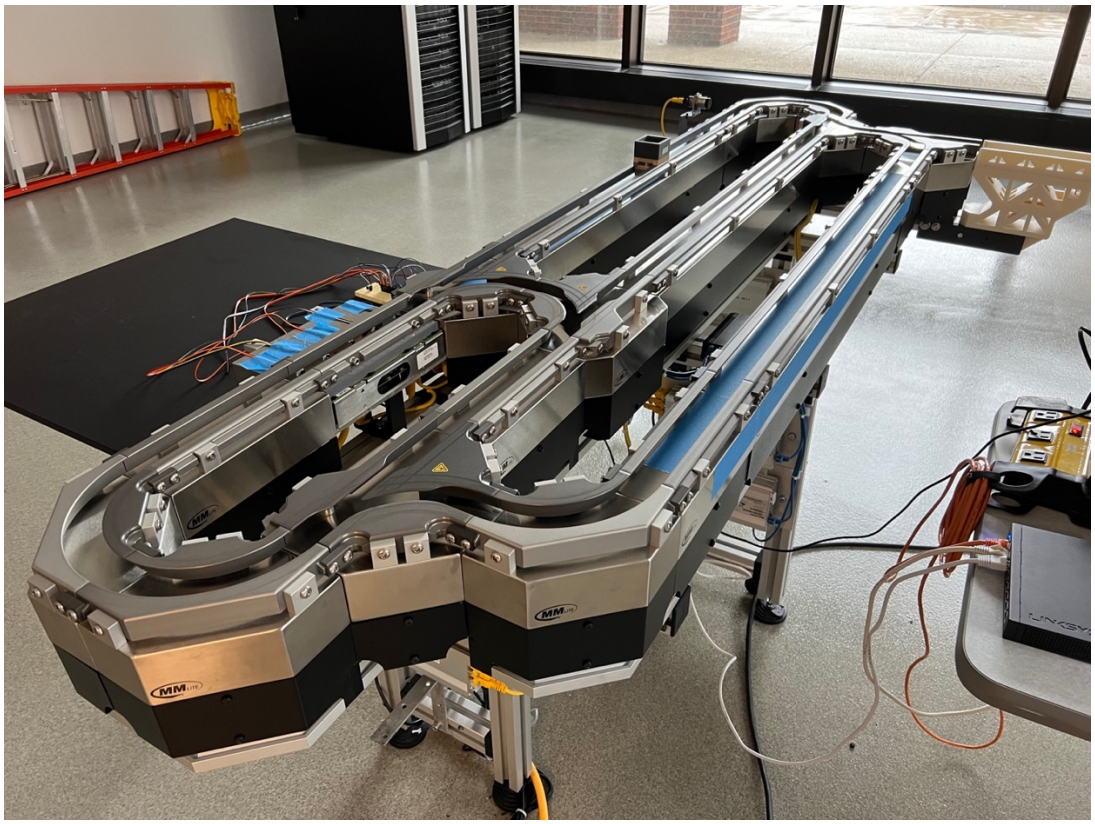

Figure 2.5 Full Physical Model of the Linear Magnetic Motors (Entire System)

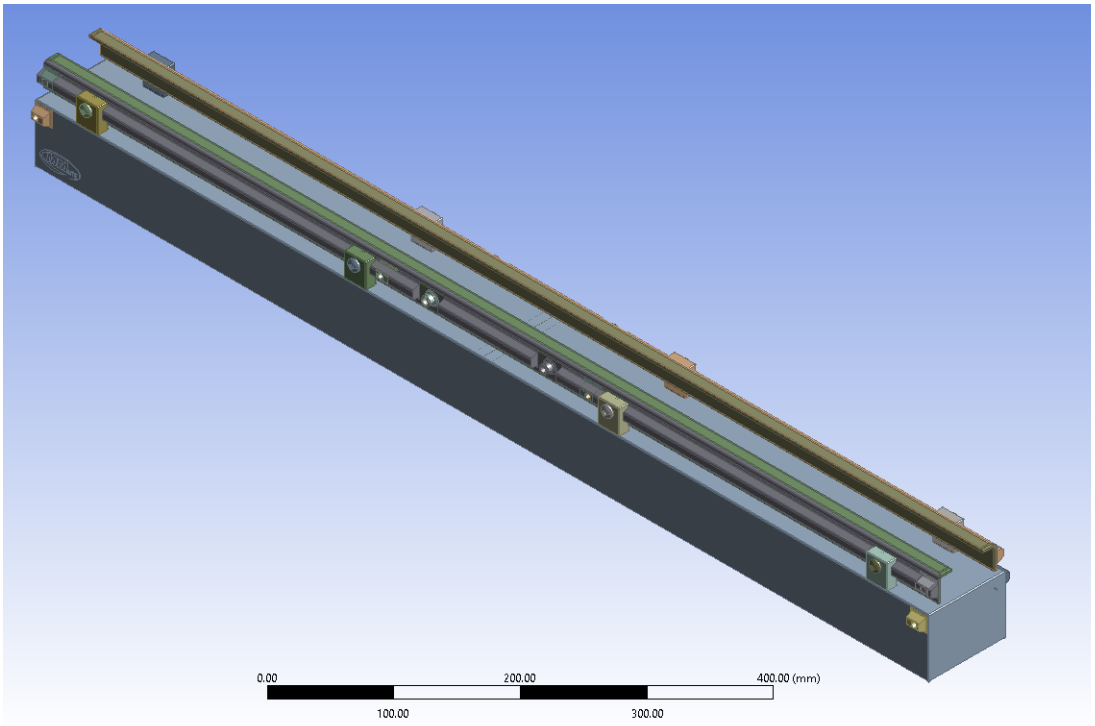

Figure 2.6 Full 3-D CAD Model of Linear Magnetic Motor (One Motor)

Although we possess the comprehensive 3-D parametric CAD model derived from the physical model, it remains imperative to conduct a meticulous analysis to determine the essential components and features for inclusion within the numerical model. Our primary focus is on understanding of thermal dynamics exhibited by the linear magnetic motor, while concurrently striving to optimize computational efficiency. To achieve this goal, we retained solely the pertinent heat source and its associated components. Therefore, system elements such as rails, covers, and screws have been intentionally excluded from the FEA geometry to streamline the model.

In alignment with these principles, our simplified numerical model exclusively incorporates the coils and EPDM Rubber, which enshrouds the coils. This abridged model, as depicted in Figure 2.7, underscores our commitment to distilling the model to its core thermal aspects, effectively prioritizing computational speed and precision.

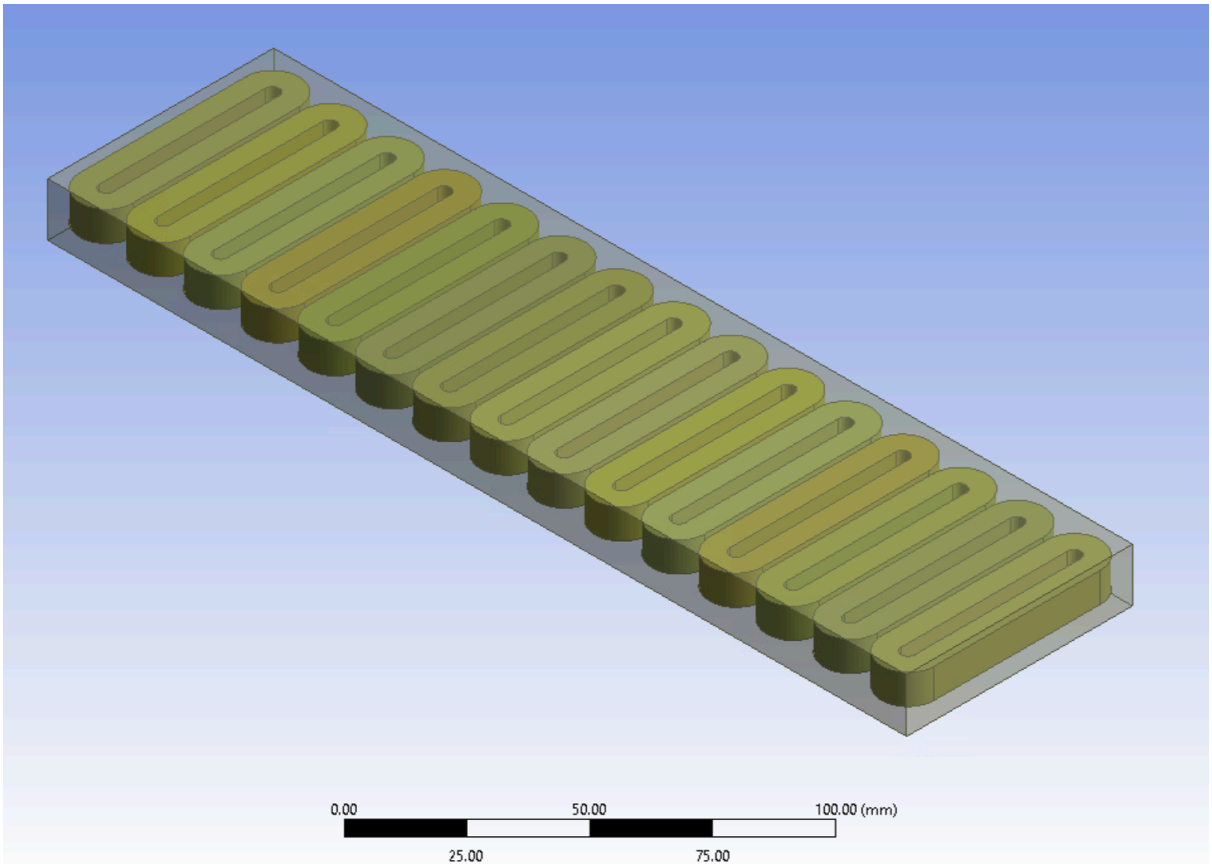

Figure 2.7 Simplified CAD Model

The Finite Element Method (FEM) is a numerical approach of choice for this project, employed to solve differential and integral equations through iterative procedures. At the heart of FEM lie its constituent elements, which are elemental building blocks fundamental to the method's operation. In our study, the transient thermal model is aptly delineated using tetrahedral elements and hexahedral elements. Tetrahedral elements and hexahedral elements, as illustrated in (Figure 2.8, Figure 2.9) [25], constitute the most widely utilized components within FEM. Their prevalence can be attributed to their remarkable capability to precisely accommodate a diverse array of curved geometries. Given their versatility and precision, we adopt tetrahedral elements as the basis for constructing our numerical model.

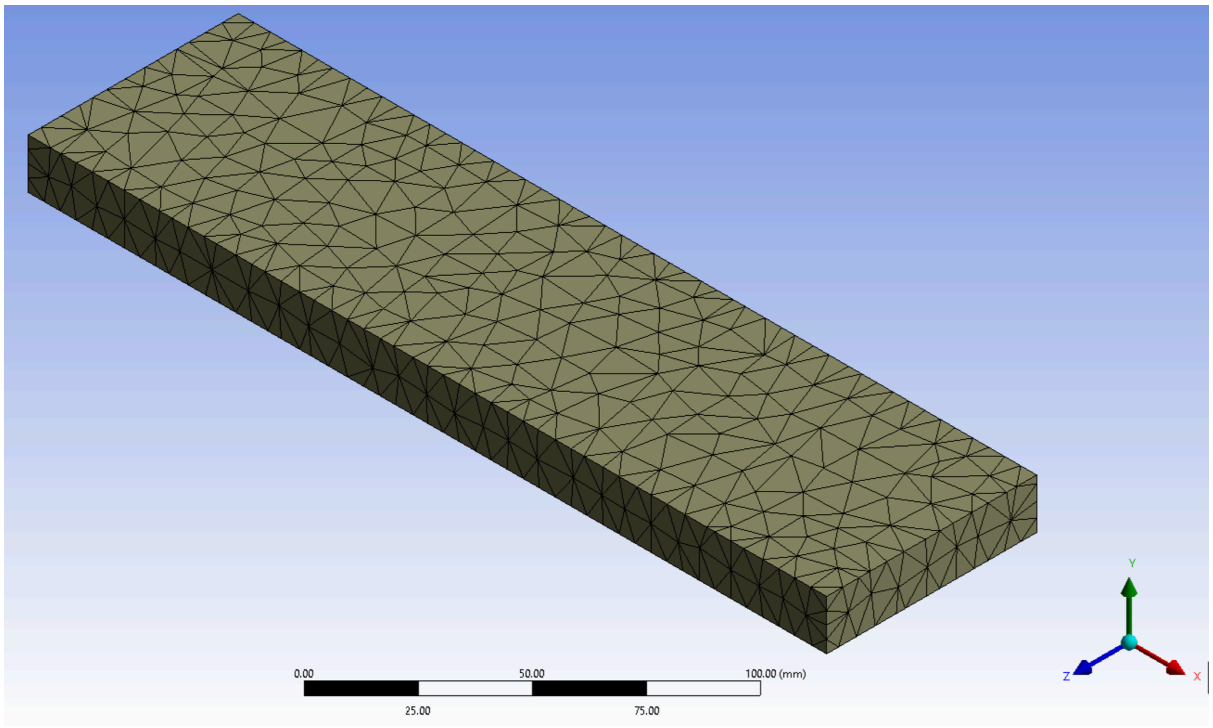

Figure 2.8 Tetrahedral Mesh of EPDM Rubber

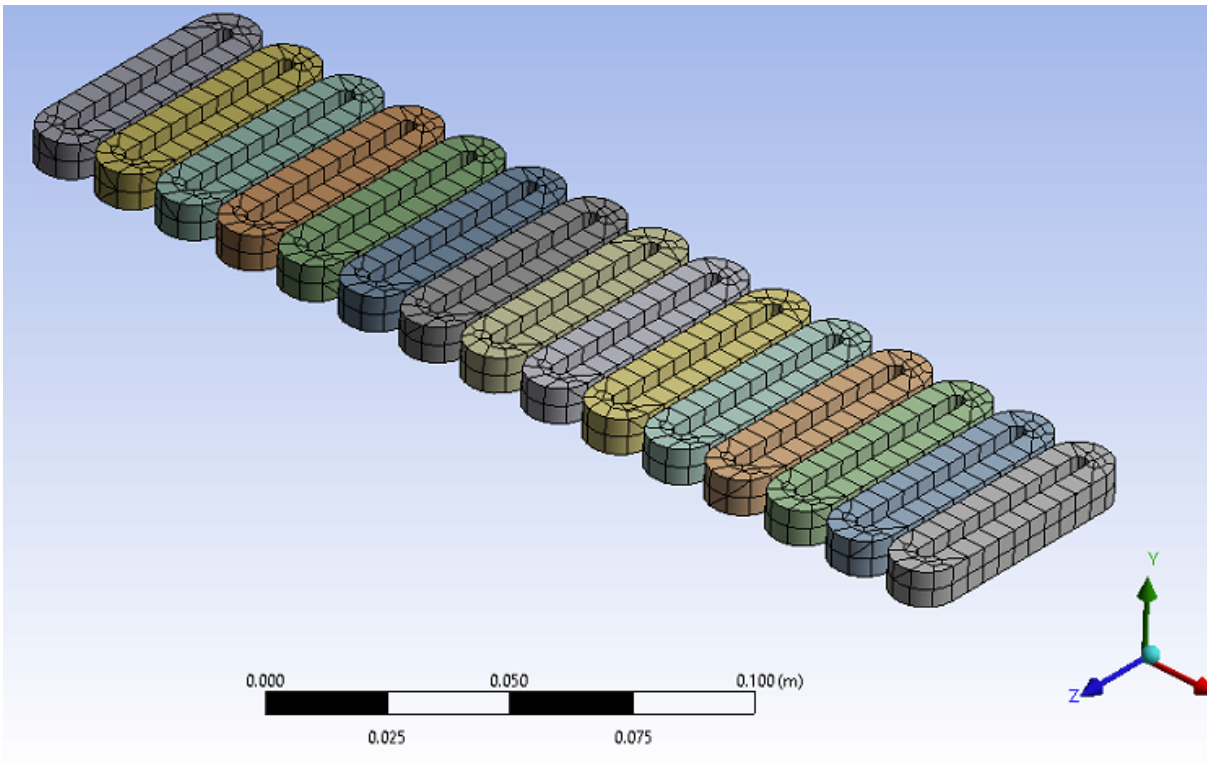

Figure 2.9 Tetrahedral and Hexahedral Mesh of Coils

After building simplified model and FE mesh, we assigned the material properties to the model components. The material properties of rubber and coils are shown in Table 2-2 and Table 2-3.

Table 2-2 Material Properties of EPDM Rubber

Properties of Outline Row 4: EPDM_Rubber

	A	B	C	D	E
1	Property	Value	Unit		
2	Material Field Variables	Table			
3	Density	1190	kg m^-3		
4	Isotropic Thermal Conductivity	0.29	W m^-1...		
5	Specific Heat Constant Pressure, C_p	1	J kg^-1 ...		

Table 2-3 Material Properties of the Coil

Properties of Outline Row 3: Copper

	A	B	C	D	E
1	Property	Value	Unit		
2	Material Field Variables	Table			
3	Density	8933	kg m^-3		
4	Isotropic Thermal Conductivity	400	W m^-1...		
5	Specific Heat Constant Pressure, C_p	385	J kg^-1 ...		

Then, we proceed to define the requisite boundary conditions for the simulation. For our transient thermal simulation, specific initial conditions are integral to solving the mathematical models effectively. These initial conditions encompass the initial temperature of the model, representative of the ambient room temperature. Additionally, we incorporate the film coefficient, signifying the convection coefficient [32], alongside the heat source parameters. For this study, the maximum power consumption is assumed to be under 35W. Furthermore, we recognize that power consumption adjusts in correspondence with the load carried by the motor during transmission. Consequently, our strategy involves executing an array of diverse scenarios, spanning power consumptions of 10W, 15W, 20W, 25W, 30W, and 35W over a time span of 6,000 seconds. These scenarios furnish a comprehensive spectrum of conditions to scrutinize.

The initial conditions and excitations integral to each of these scenarios are systematically documented Table 2-4. Of particular interest is the 35W scenario, which represents an extreme operational case for the motor. This comprehensive approach allows us to thoroughly investigate the thermal behavior across a spectrum of conditions, enriching our understanding of the system's dynamics.

Table 2-4 Initial Conditions and Boundary Conditions

Index	Ambient Temperature (°C)	Film Coefficient ($W/m^2*°C$)	Power Consumption (W)
1	22	25	10
2	22	25	15
3	22	25	20
4	22	25	25
5	22	25	30
6	22	25	35

2.4 Reduced-Order Modeling

Despite the continuous advancement of High-Performance Computing (HPC) systems, the computational demands of such intricate models remain time intensive. To expedite the simulation process, we employ the dynamic Reduced-Order Modeling (ROM) method, leveraging the capabilities of ANSYS Dynamic ROM Builder. This innovative approach involves utilizing 3-D simulation results as the output data, coupled with excitation data serving as the input.

The process of generating the ROM follows a systematic workflow, as depicted in Figure 2.10. This strategy enables us to effectively distill the complexity of the model while retaining the essential dynamics, thereby significantly reducing computational time, and enhancing efficiency.

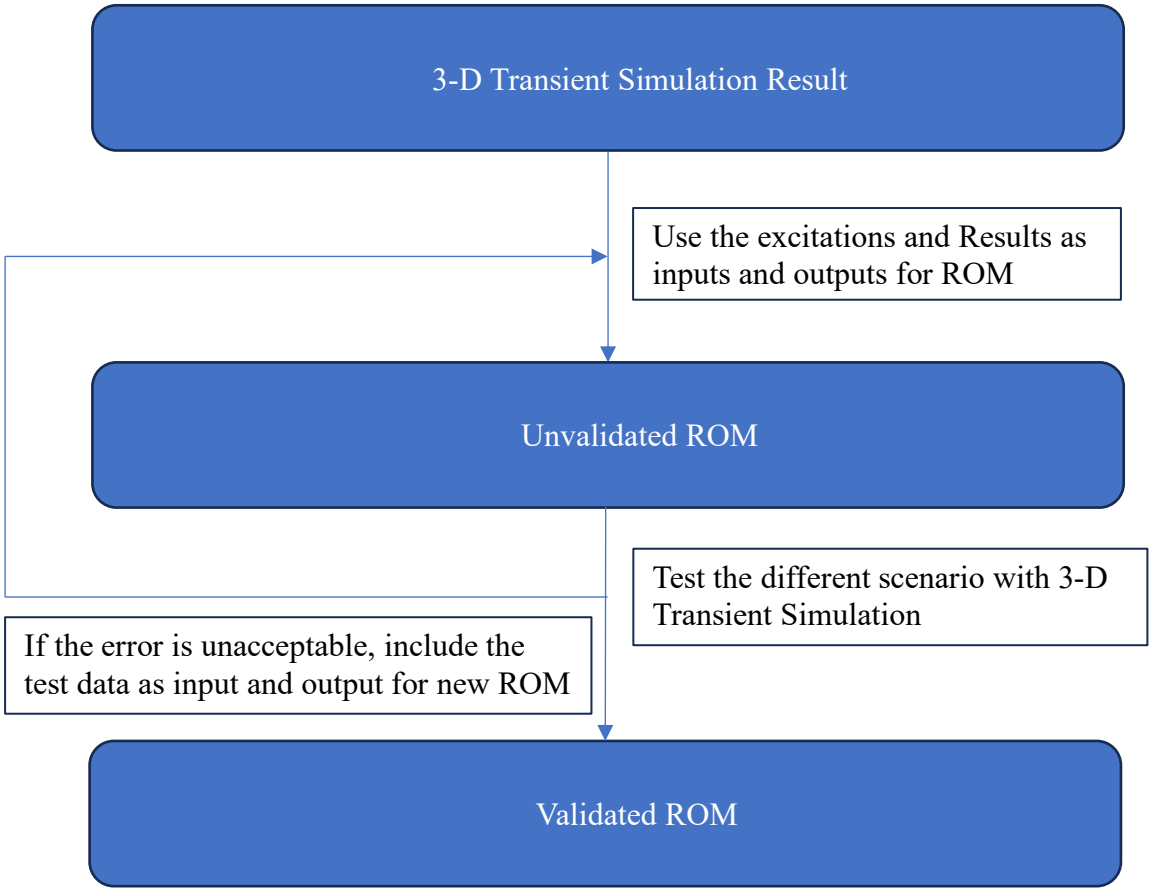

Figure 2.10 The Workflow of Building a Dynamic Reduced-Order Model

As detailed in the ANSYS Twin Builder User Help Manual [30], the foundation of the Dynamic Reduced-Order Modeling (ROM) approach is rooted in the principles of deep learning [31]. The fundamental architecture of a deep learning model comprises distinct layers: an input layer, one or more hidden layers, and an output layer. The input values are initially assigned random weight coefficients and biases. Progressing through the hidden layer(s), the values at the final layer are derived as a summation of the weighted values from the preceding layer, subsequently undergoing activation through an activation function, yielding the output value. This sequence is commonly referred to as "forward propagation."

After forward propagation, optimization techniques are employed to fine-tune the initially randomized weight coefficients, aiming to enhance accuracy or computational

efficiency. This iterative procedure is denoted as "backward propagation." A graphical depiction of a single-layer neural network is depicted in Figure 2.11, illustrating the intricate mechanics of this deep learning framework.

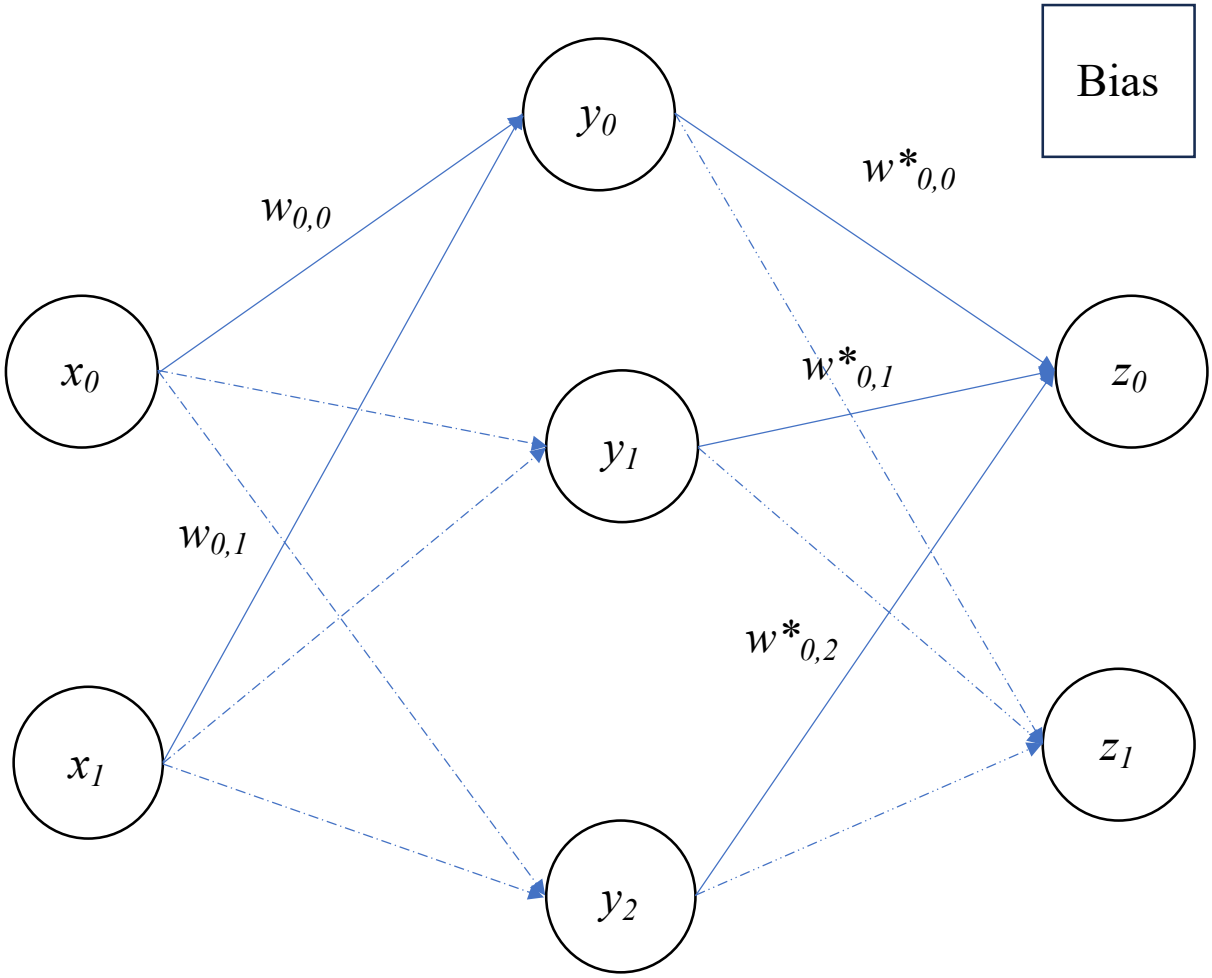

Figure 2.11 Single-Layer Neural Network

Let's consider a brief example for the concept of deep learning. Here: x_0 is one of the input values from the user. Then we multiply the input value by the random weight coefficient ($w_{i,j}$), so we could obtain function $y_{i,j}$:

$$y_0 = x_0 w_{0,0} + x_1 w_{0,1} \tag{2.4}$$

Then, after calculating y_j, we could use the same principle to get the value which we should apply in activation function to obtain the output value:

$$z_0 = A(y_0 w^*_{0,0} + y_1 w^*_{0,1} + y_2 w^*_{0,2} + Bias) \tag{2.5}$$

Where: A(z) is the activation function

Then, after finishing the process of forward propagation and getting the value from the output layer we could use the backward propagation to compute new weight coefficients. In the process of backward propagation, we calculate the loss function, C(w) and its gradient used to update weight coefficients:

$$C(w) = \frac{\Sigma(w - \widetilde{w})^2}{n} \tag{2.6}$$

$$w_{new} = w_{old} - \eta * \nabla C\left(w_{i,j}, w^*_{i,j}\right) \tag{2.7}$$

Where: η is the learning rate which is a tuning parameter for optimizing the result.

By employing this conceptual framework, we can continually refine our deep learning model through training across diverse scenarios, aiming to attain an increasingly time-efficient and accurate dynamic reduced-order model. In the context of our current study, our primary focus is directed towards comprehending the thermal dynamics exhibited by the linear magnetic system, with specific emphasis on the temperature distribution across the motor's surface.

To achieve this objective, we use a range of power inputs, extracted from the 3-D simulations, as the excitation signals for our dynamic Reduced-Order Model (ROM). Meanwhile, the temperature distribution data, derived from the 3-D simulations, serves as the corresponding output data for our dynamic ROM. This strategy effectively equips us with a

predictive tool that accurately captures and expedites the system's thermal behavior, enabling us to make informed analyses of temperature profiles across the motor's surface.

2.5 Experimental Setup for Data Acquisitions

As per the *MagneMover Lite* user manual [26], the maximum allowable number of 62 mm vehicles (pucks) per meter is capped at 9 pucks at a time. These vehicles can achieve a top speed of 2 meters per second and a maximum acceleration of 9.0 m/sec² [26]. Armed with these insights, it's evident that the worst-case scenario unfolds when the motor operates at its peak speed and acceleration. To gauge the potential impact on operational temperature, an experiment is devised to monitor the maximum temperature attained when the *MagneMover Lite* is subjected to the highest speed and acceleration settings.

For this experiment, the data acquisition system comprises an Arduino Uno and LM35 temperature sensors. The Arduino Uno is an open-source embedded system hardware platform, offering a versatile avenue for crafting interactive projects. Meanwhile, the LM35 sensor is an integrated-circuit temperature sensor with a linearly proportional output voltage corresponding to centigrade temperature [27]. Six LM35 sensors are employed, with one dedicated to measuring room temperature and the remaining five evenly distributed along the motor's top surface.

The schematic representation of this setup is illustrated in Figure 2.12, while the experimental arrangement is depicted in Figure 2.13. These elements collectively constitute the experimental framework employed to investigate the temperature variations when the *MagneMover Lite* is subjected to its utmost operational speed and acceleration conditions.

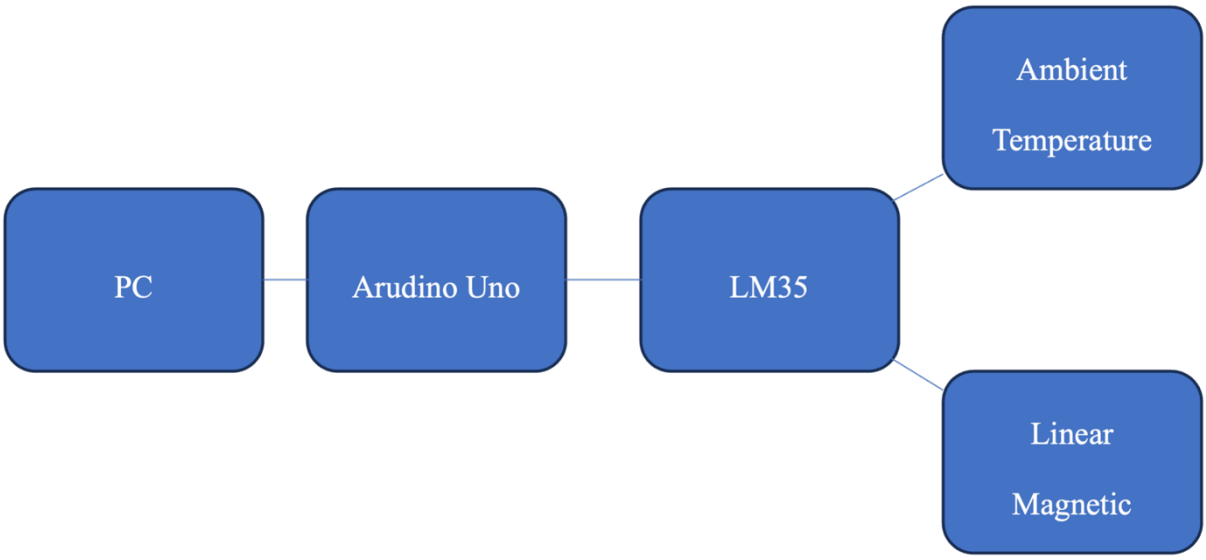

Figure 2.12 The Schematics of Data Acquisition Process

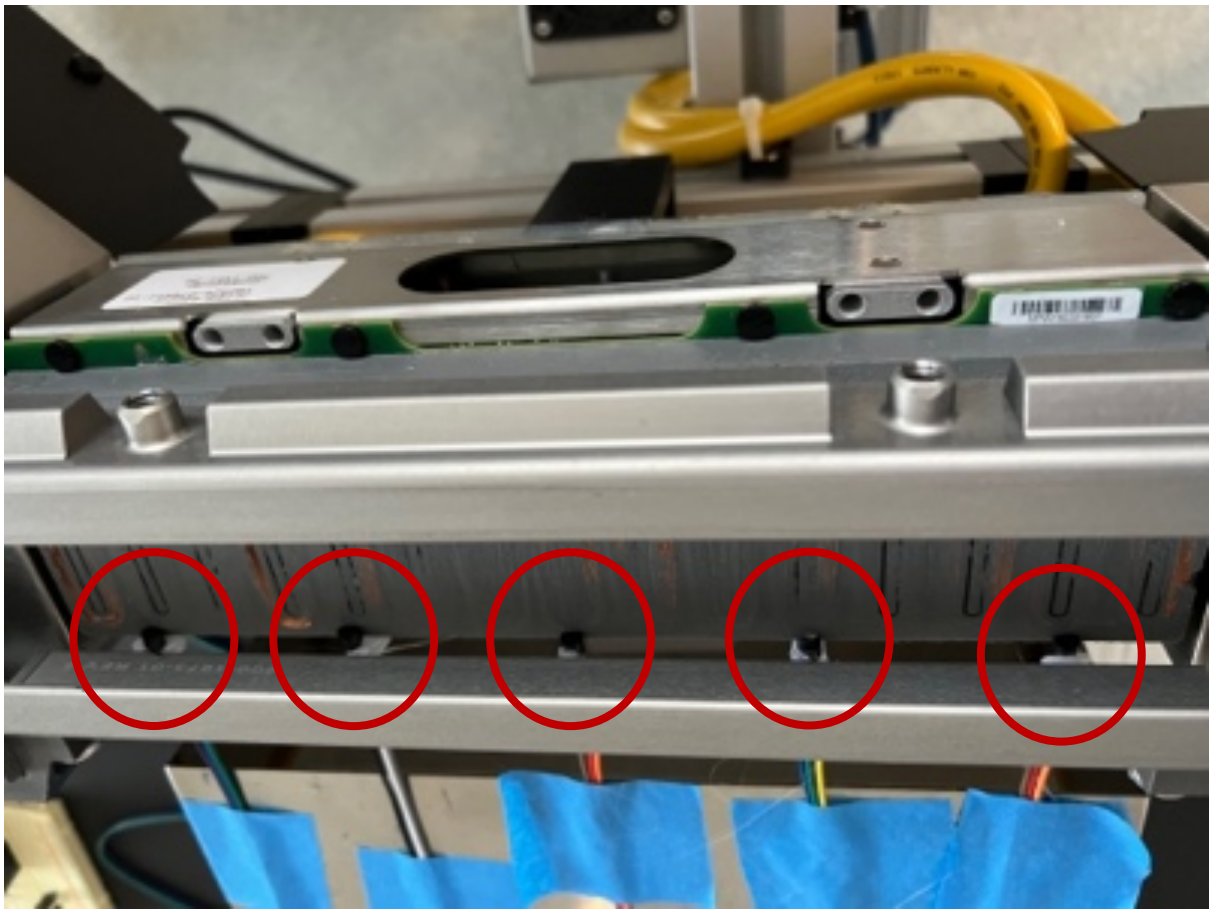

Figure 2.13 The Experimental Setup: Temperature Sensors' Placement

3. Results

3.1 Numerical Convergence Test

This chapter will comprehensively present the outcomes derived from the 3-D simulation, dynamic ROM, and experimental study. However, prior to delving into the intricacies of the 3-D simulation, a pivotal preliminary step involves assessing the adequacy of the number of elements employed in constructing the numerical model. To ascertain this, we undertake a mesh convergence test.

In this test, we meticulously evaluate the impact of varying mesh lengths, specifically analyzing four distinct mesh lengths: 10mm, 7.5mm, 5mm, and 2.5mm. The ensuing disparities observed across these diverse mesh configurations are vividly illustrated in Figure 3.1. This iterative process aids us in establishing the optimal mesh length, crucial for ensuring the precision and reliability of our numerical model.

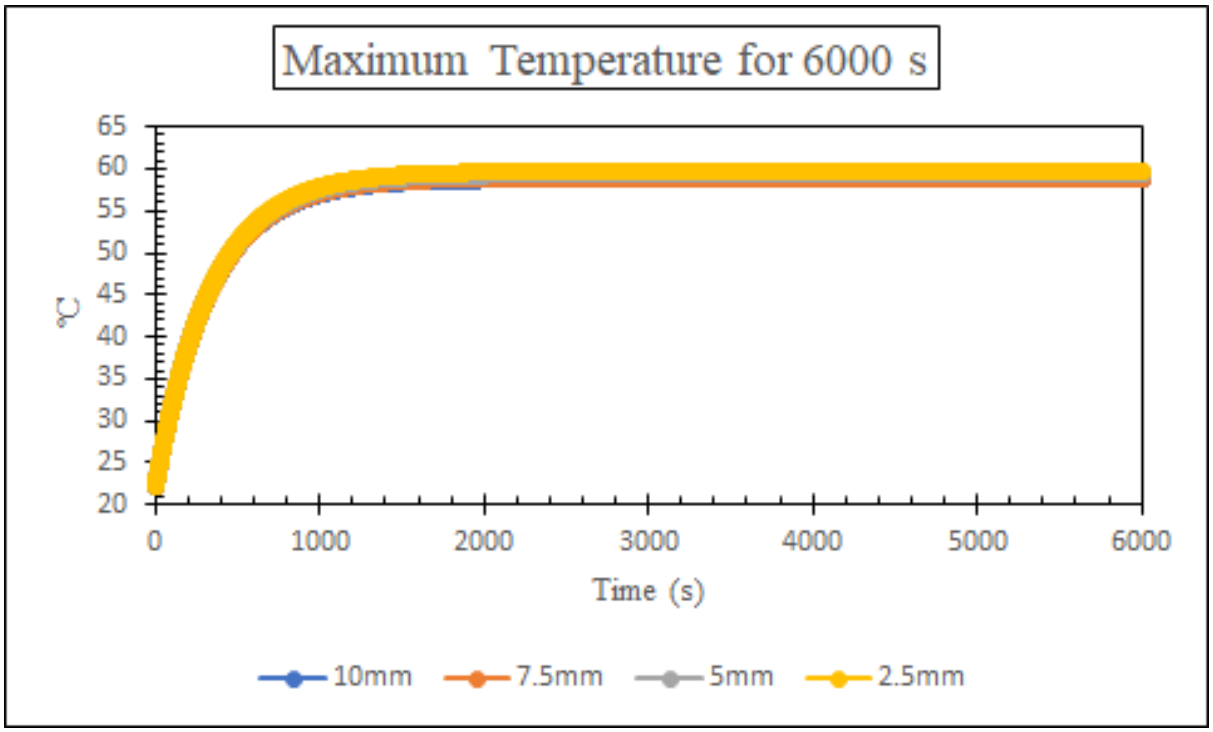

Figure 3.1 Maximum Temperatures between Four Difference Mesh Sizes

Upon conclusion of the mesh convergence test, we decided to use 5mm as the mesh size for subsequent simulations. The simulations differences among four mesh size models are shown in Figure 3.2 and undershooting of 10 mm and 7.5 mm are shown in Figure 3.3 and Figure 3.4.

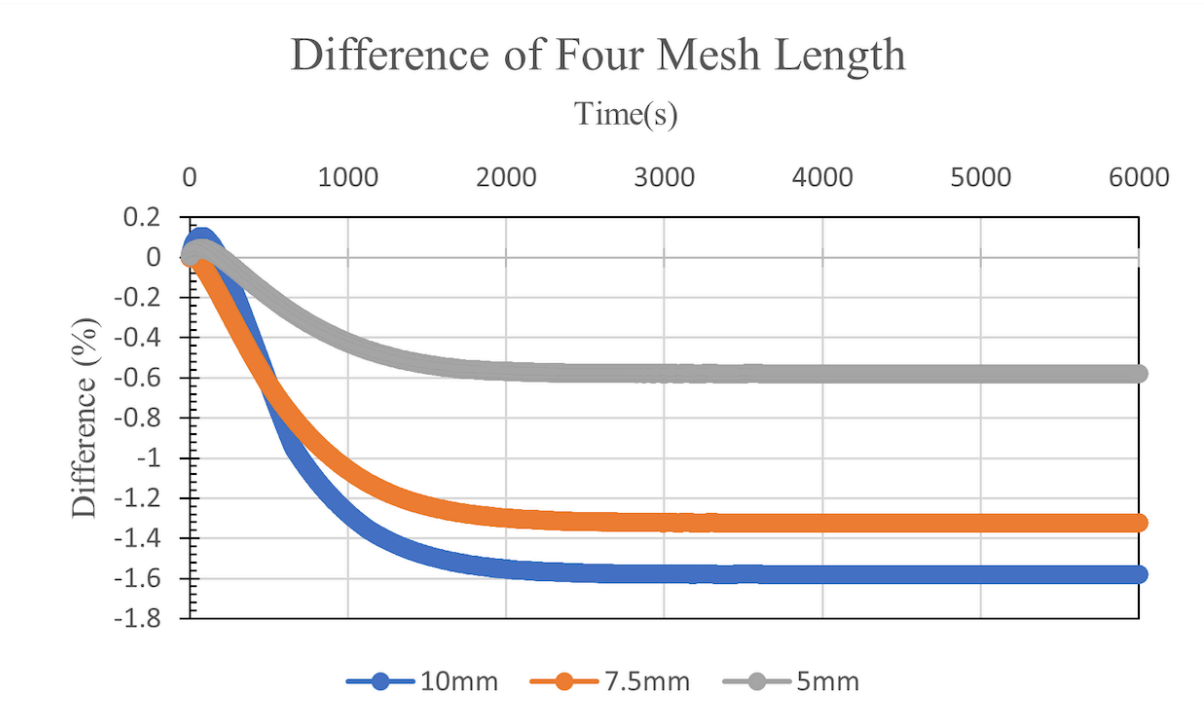

Figure 3.2 The Difference of Four Meshes

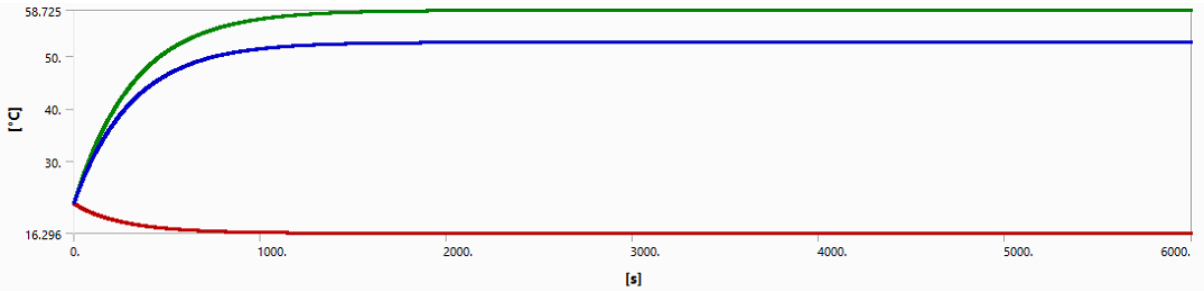

Figure 3.3 Undershooting of 10mm Meshes

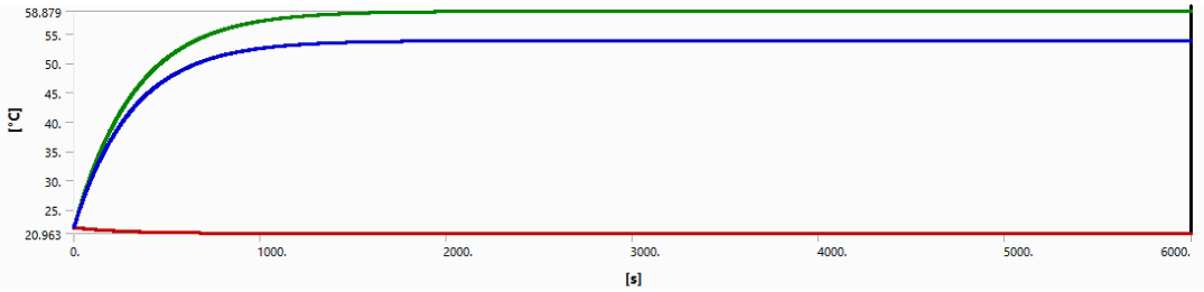

Figure 3.4 Undershooting of 7.5mm Meshes

3.2 3-D Simulation Results

Having successfully completed the mesh convergence test, we are now poised with a robust foundation to proceed with running the simulations encompassing the six distinct scenarios elucidated in Chapter 3. The outcomes stemming from the simulations conducted at power levels of 10W, 15W, 20W, 25W, and 30W are succinctly depicted in in Figure 3.5 through Figure 3.16. These visual representations serve as a comprehensive look at the thermal behaviors exhibited within the linear magnetic system across varying operational conditions.

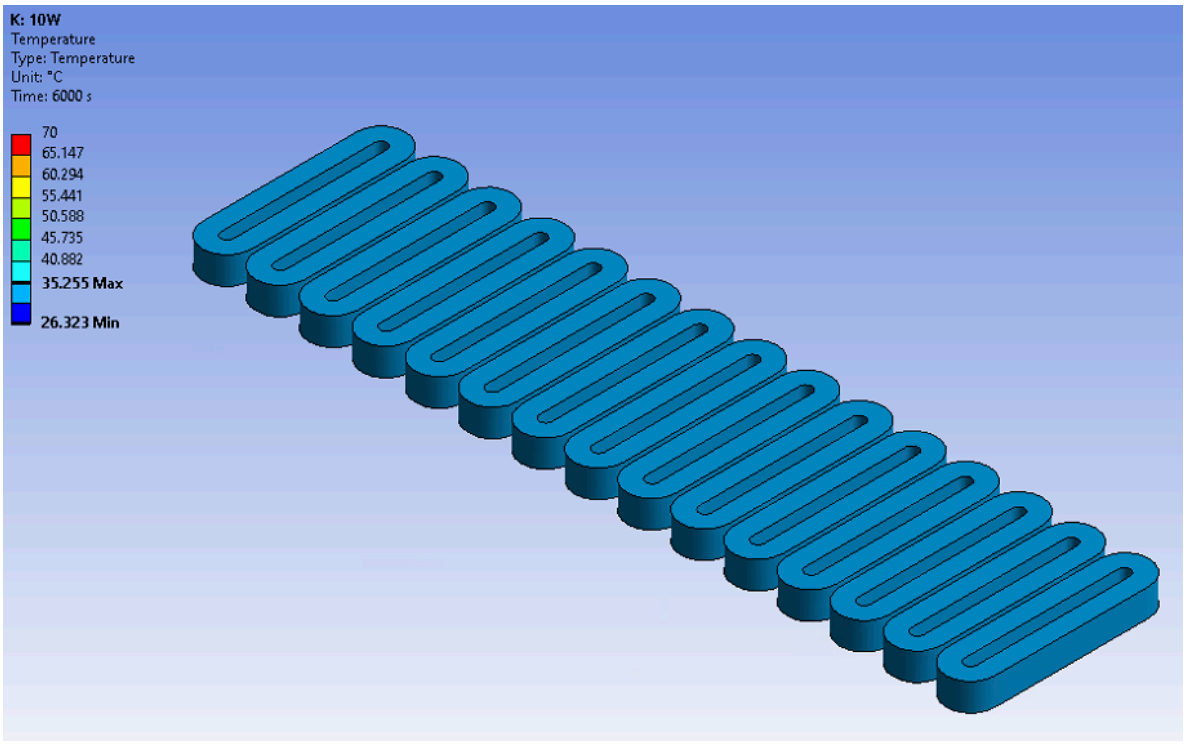

Figure 3.5 The Temperature Distribution on Coils with 10W Load

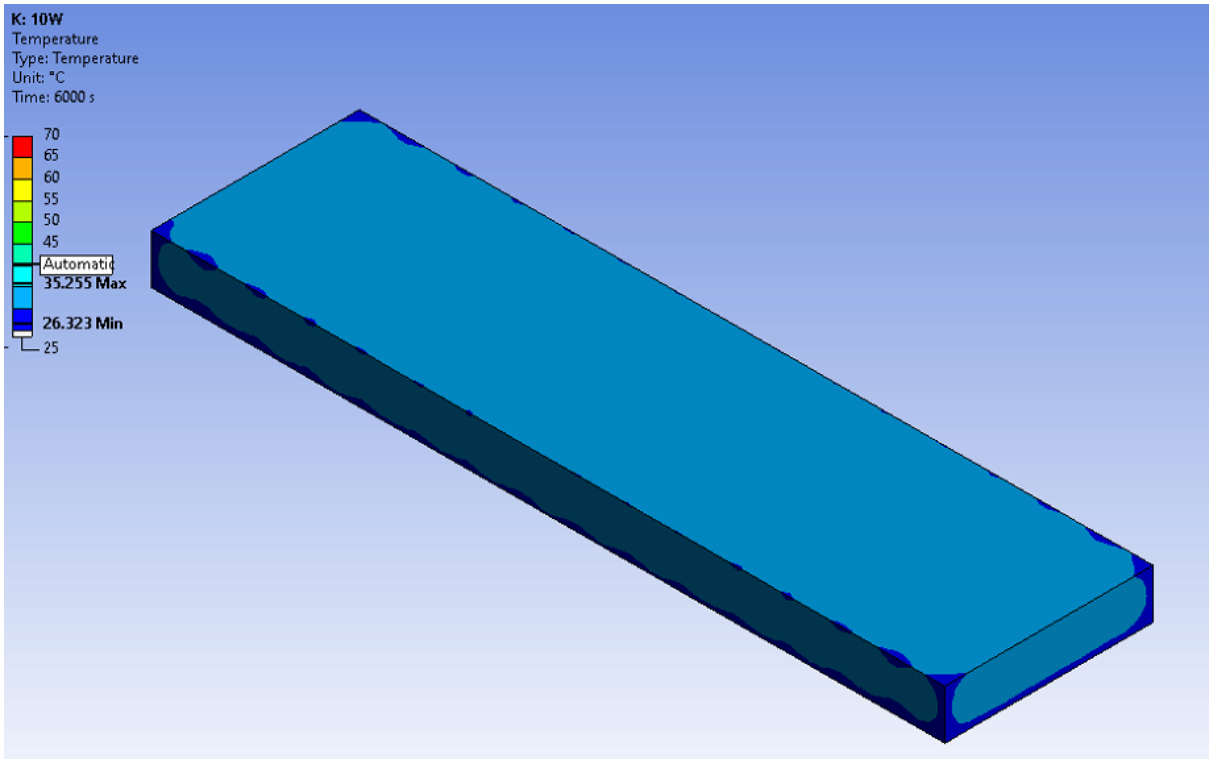

Figure 3.6 The Temperature Distribution on Wrap (EPDM Rubber) with 10W Load

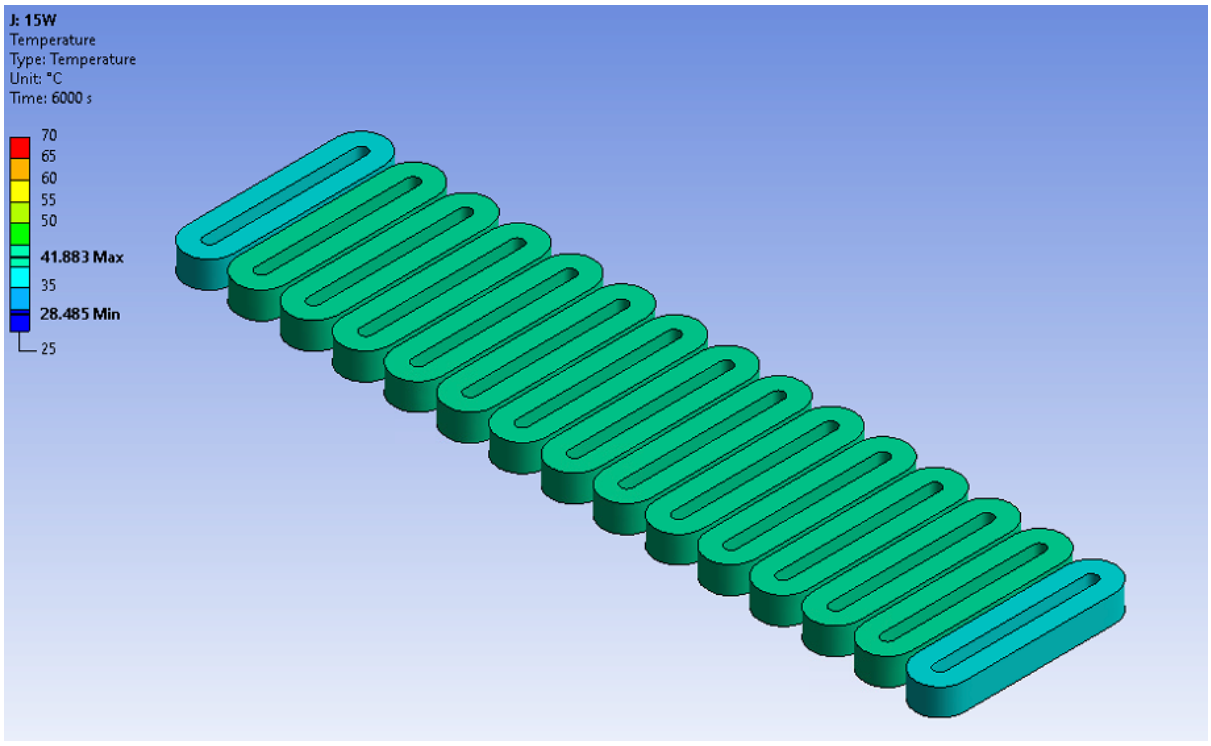

Figure 3.7 The Temperature Distribution on Coils with 15W Load

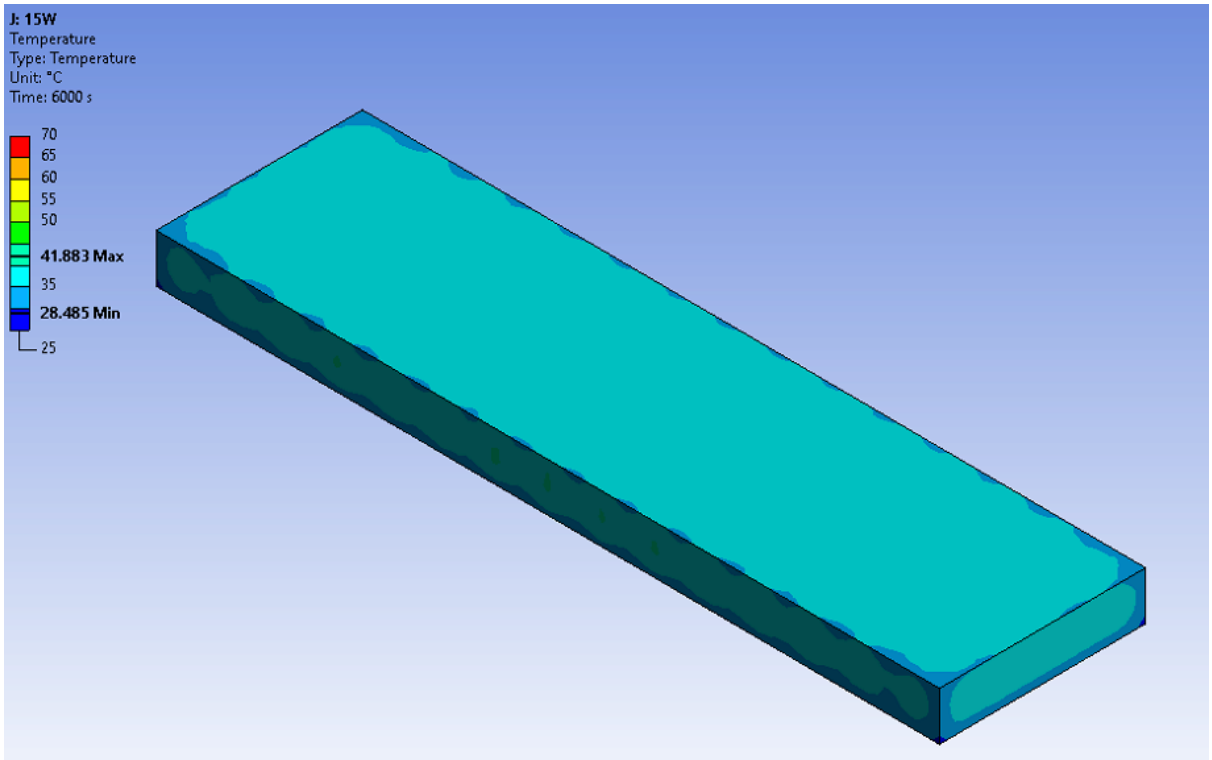

Figure 3.8 The Temperature Distribution on Wrap (EPDM Rubber) with 15W Load

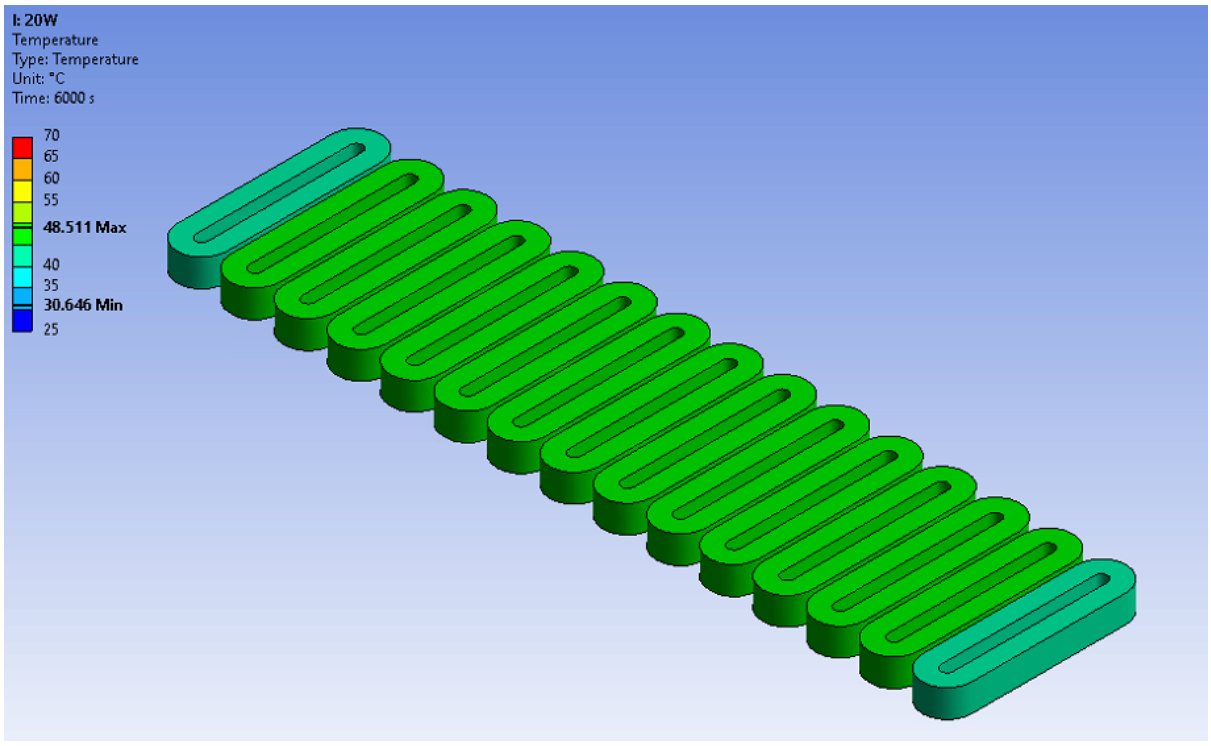

Figure 3.9 The Temperature Distribution on Coils with 20W Load

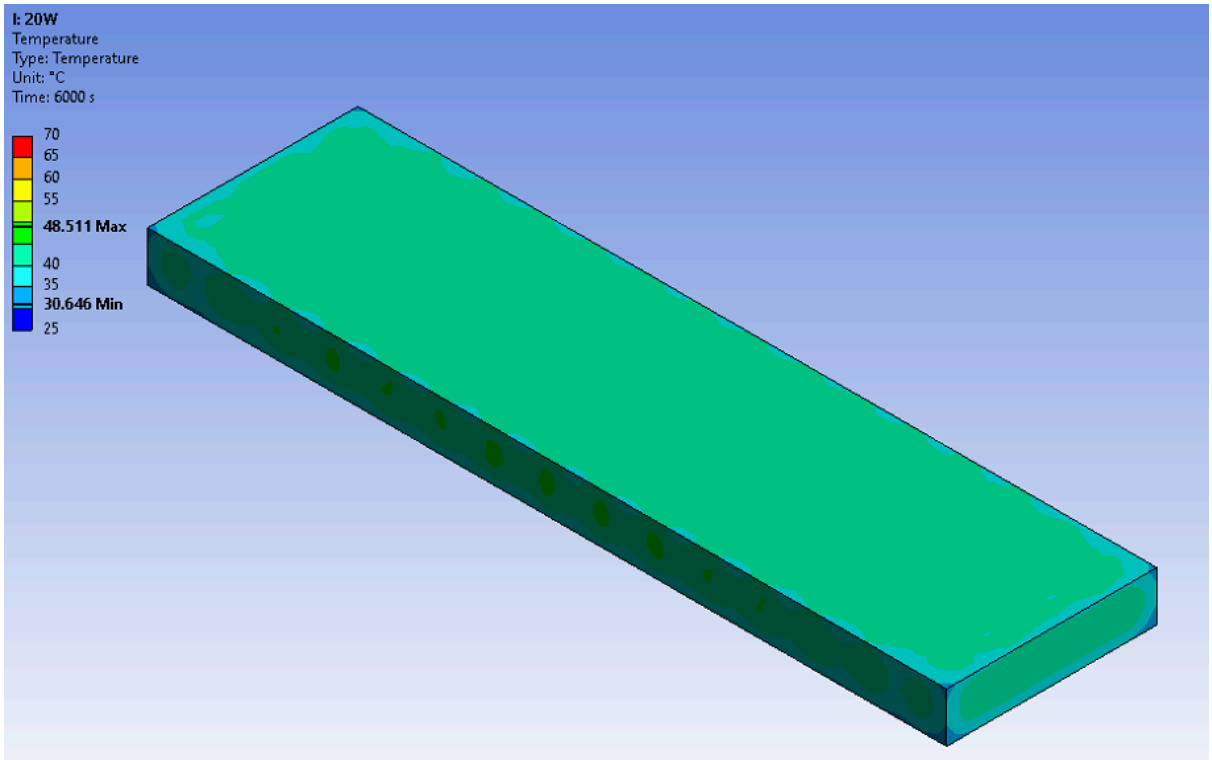

Figure 3.10 The Temperature Distribution on Wrap (EPDM Rubber) with 20W Load

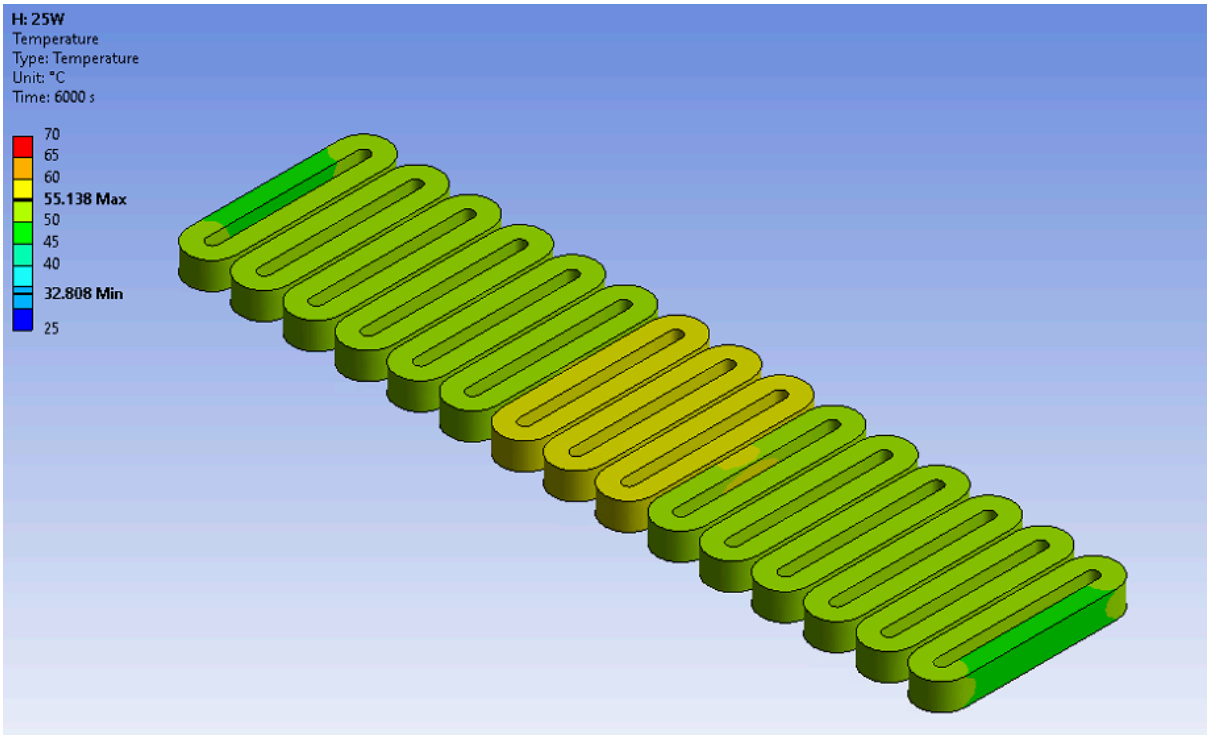

Figure 3.11 The Temperature Distribution on Coils with 25W Load

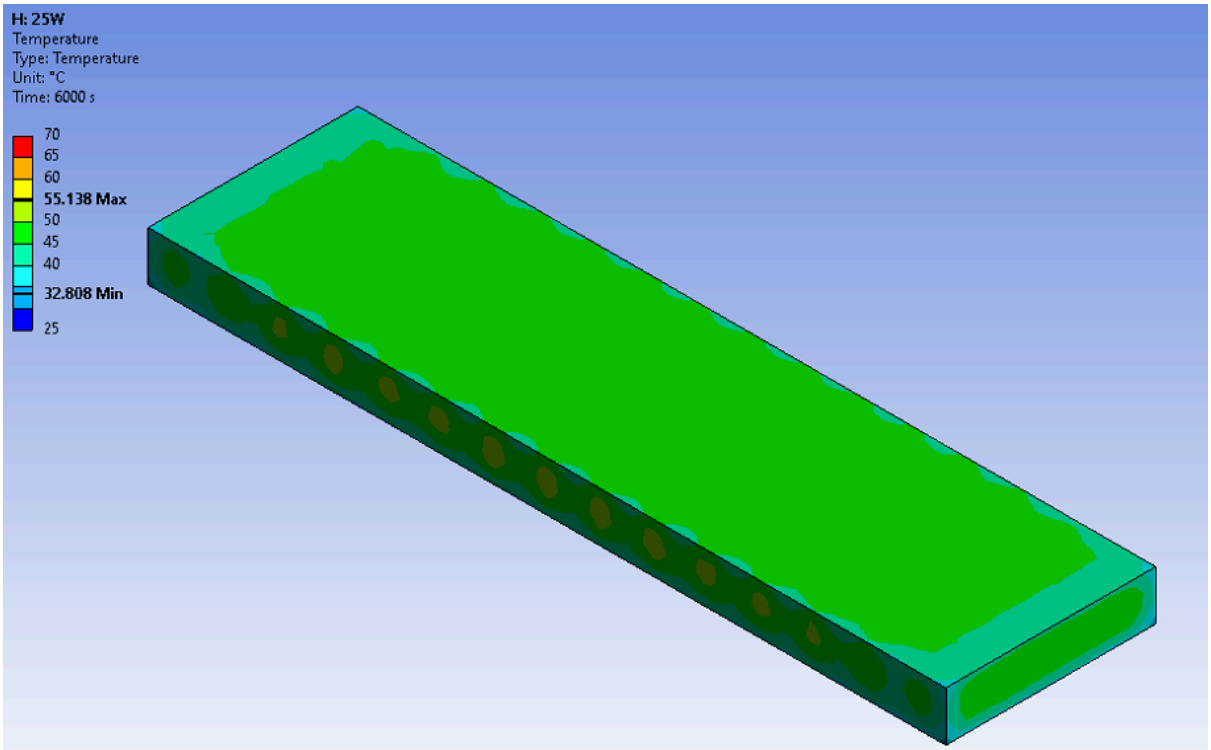

Figure 3.12 The Temperature Distribution on Wrap (EPDM Rubber) with 25W Load

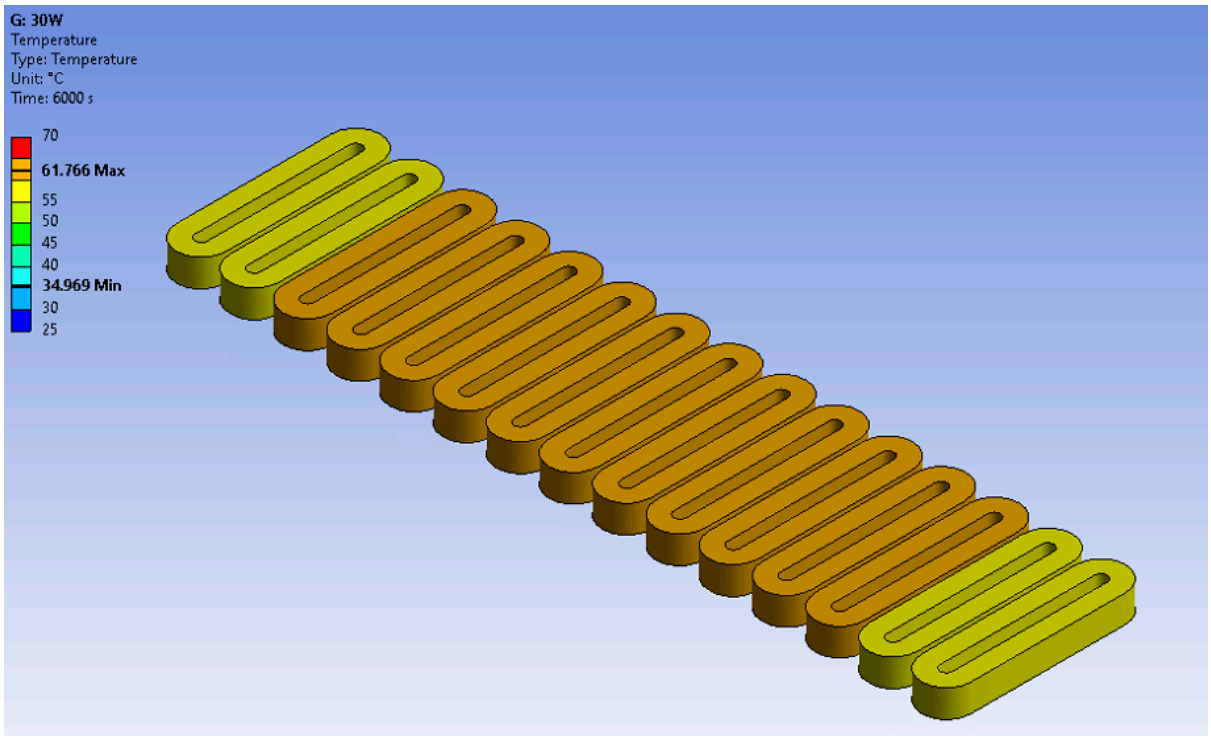

Figure 3.13 The Temperature Distribution on Coils with 30W Load

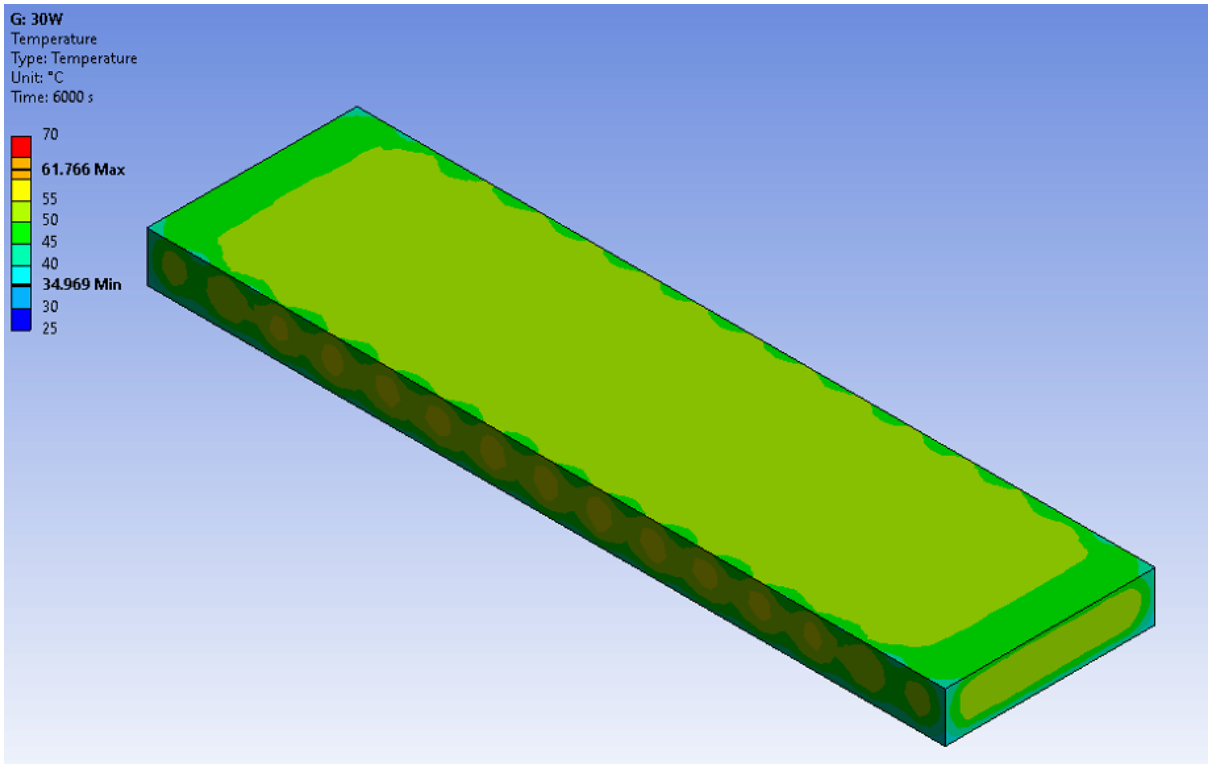

Figure 3.14 The Temperature Distribution on Wrap (EPDM Rubber) with 30W Load

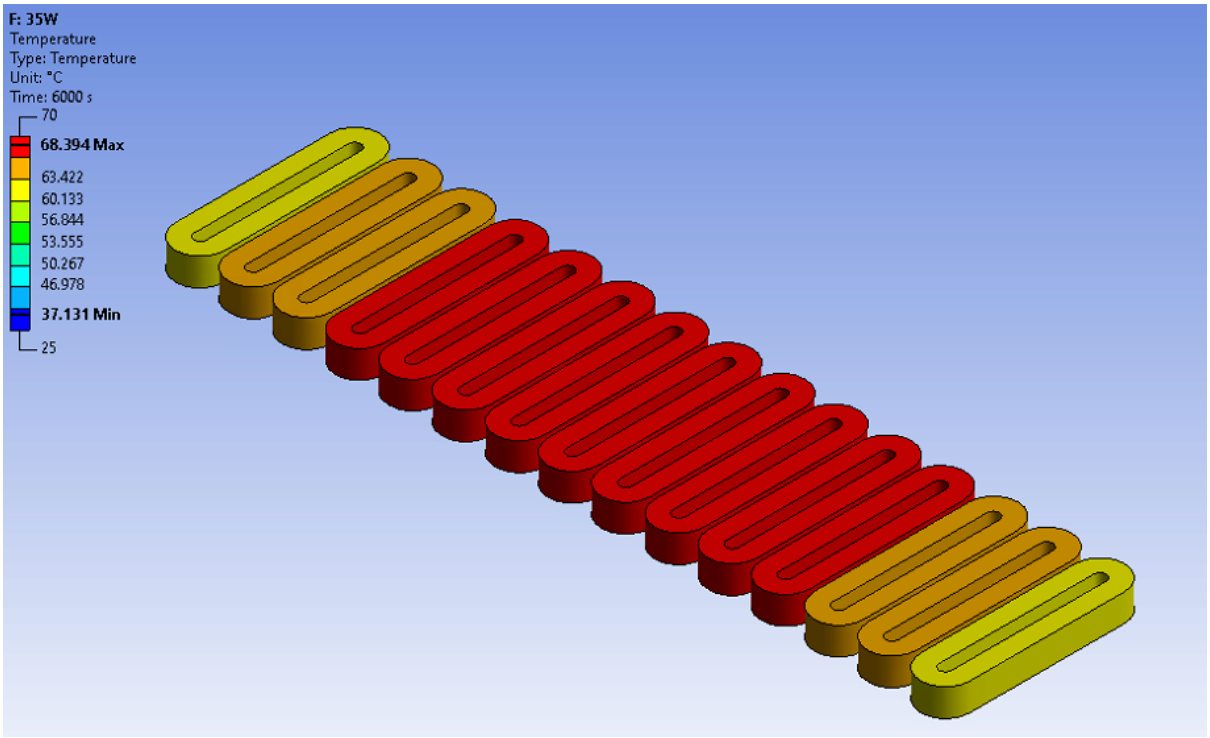

Figure 3.15 The Temperature Distribution on Coils with 35W Load

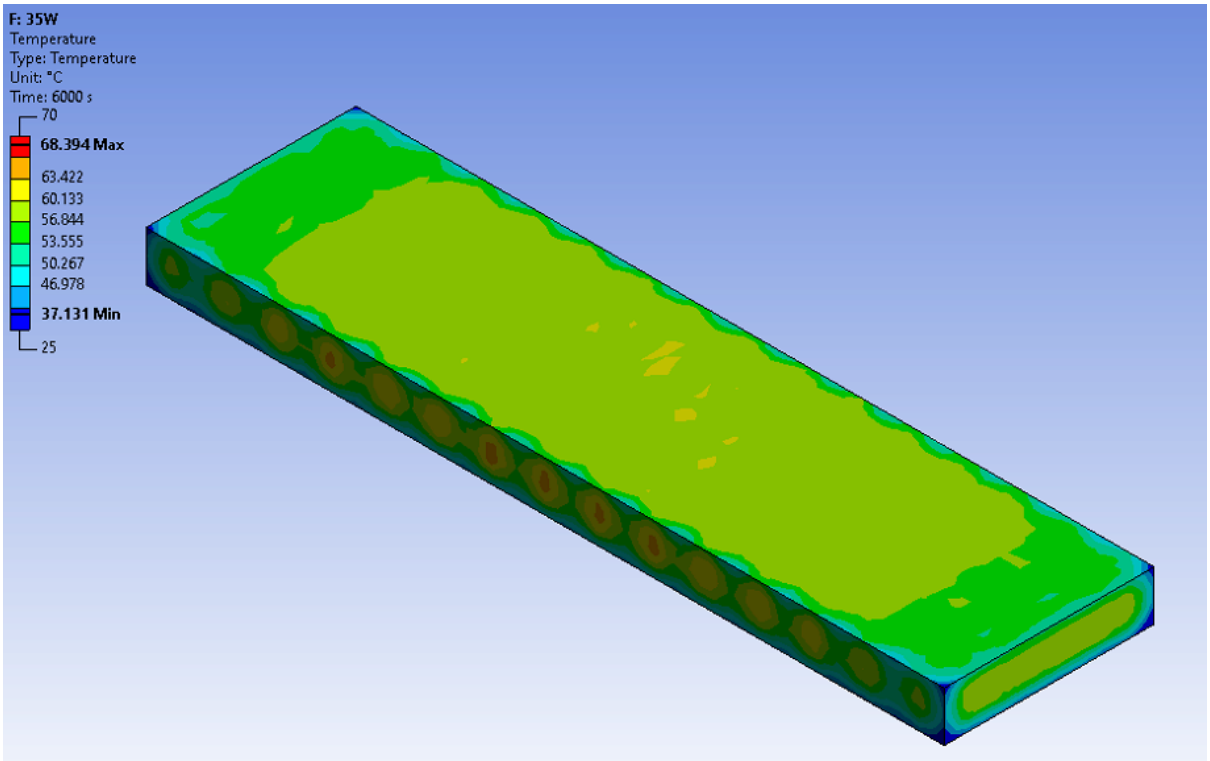

Figure 3.16 The Temperature Distribution on Wrap (EPDM Rubber) with 35W Load

3.3 Reduced-Order Modeling Results

With the amalgamation of the six distinct scenarios presented earlier, our study encompasses a total of six diverse learning scenarios for the dynamic Reduced-Order Model (ROM) to acquire insights from. Subsequently, these acquired insights are employed to predict and reproduce the system's behavior under differing conditions. These results, encompassing a comprehensive array of thermal dynamics, are succinctly displayed in Figure 3.17 through Figure 3.19.

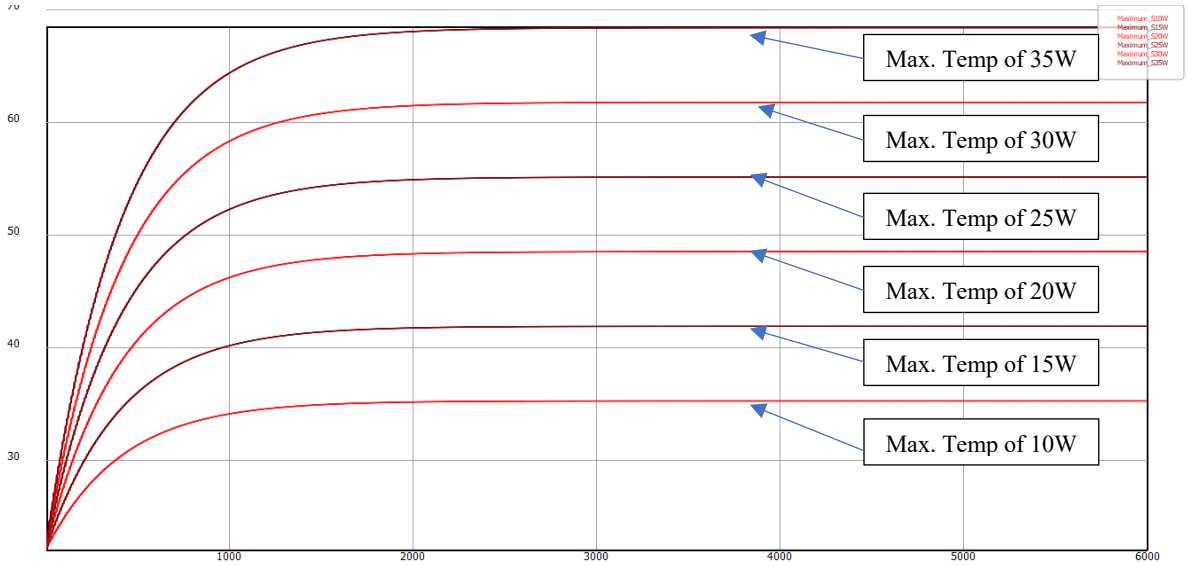

Figure 3.17 The Result from 3-D Simulation

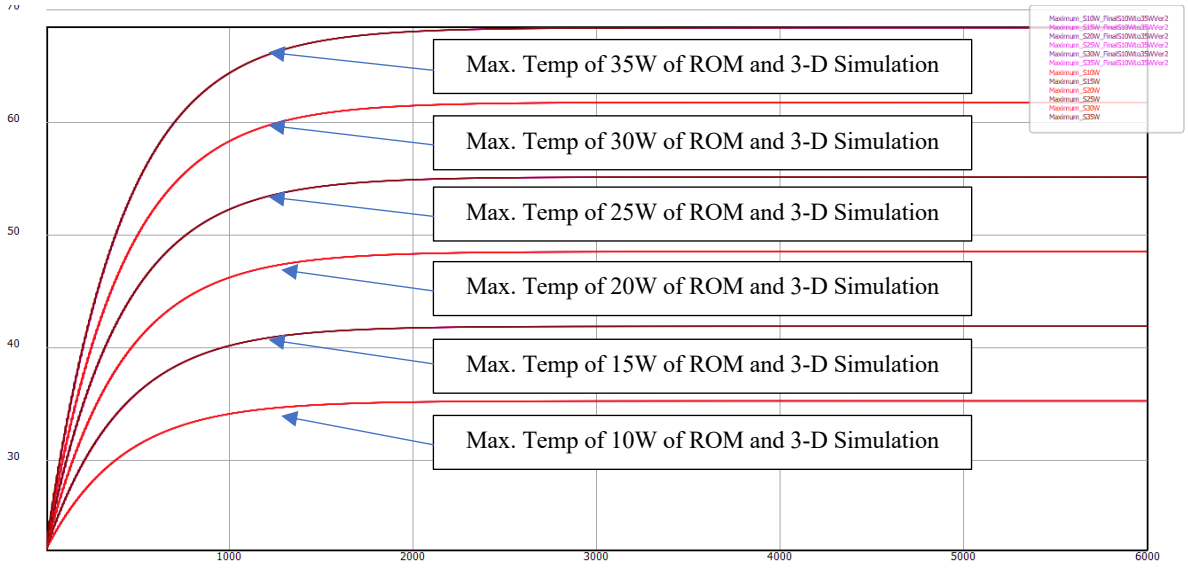

Figure 3.18 The Result of 3-D Simulations and ROMs

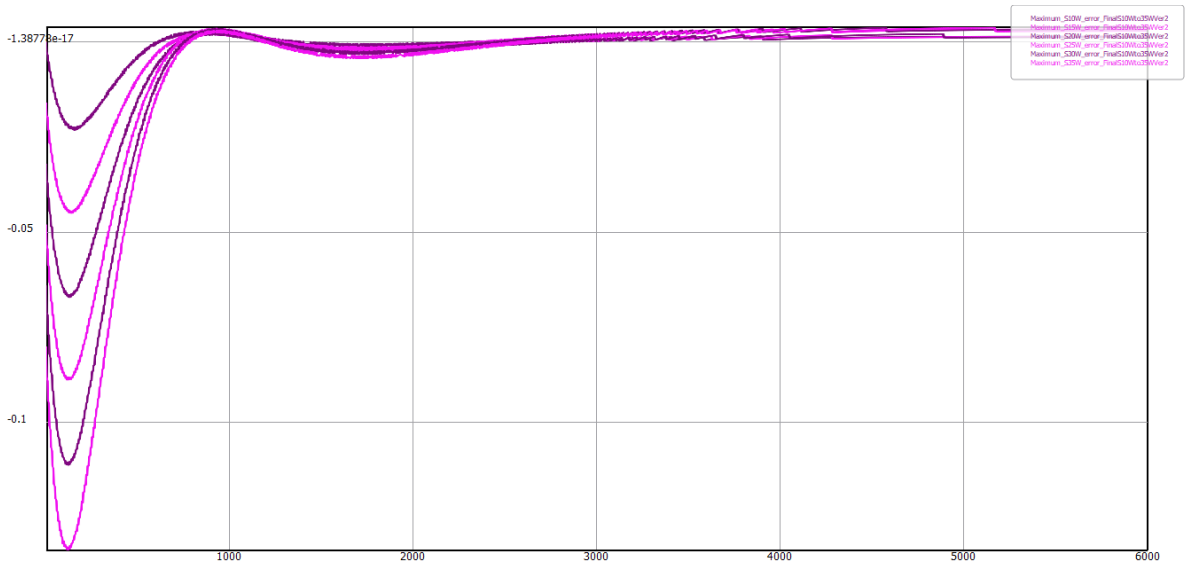

Figure 3.19 The Errors between 3-D Simulations and ROMs

Then, due to the errors between 3-D models and ROMs are less than 0.2%, we now test the ROM with a new data set from 3-D model to see if the ROM performs properly. The testing results are shown in Figure 3.20 to Figure 3.22.

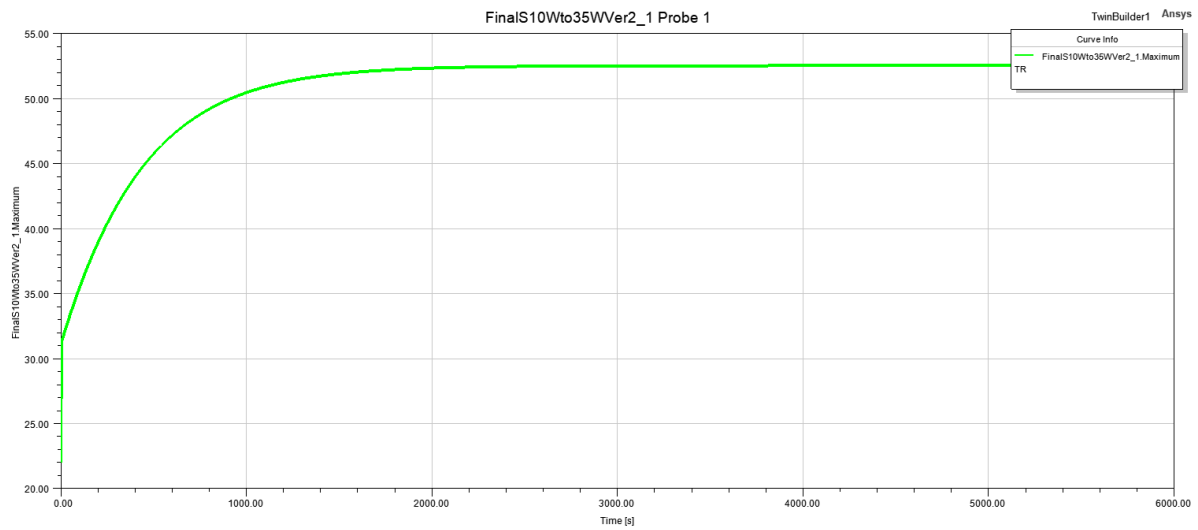

Figure 3.20 The Testing Result of ROM with 23W Load

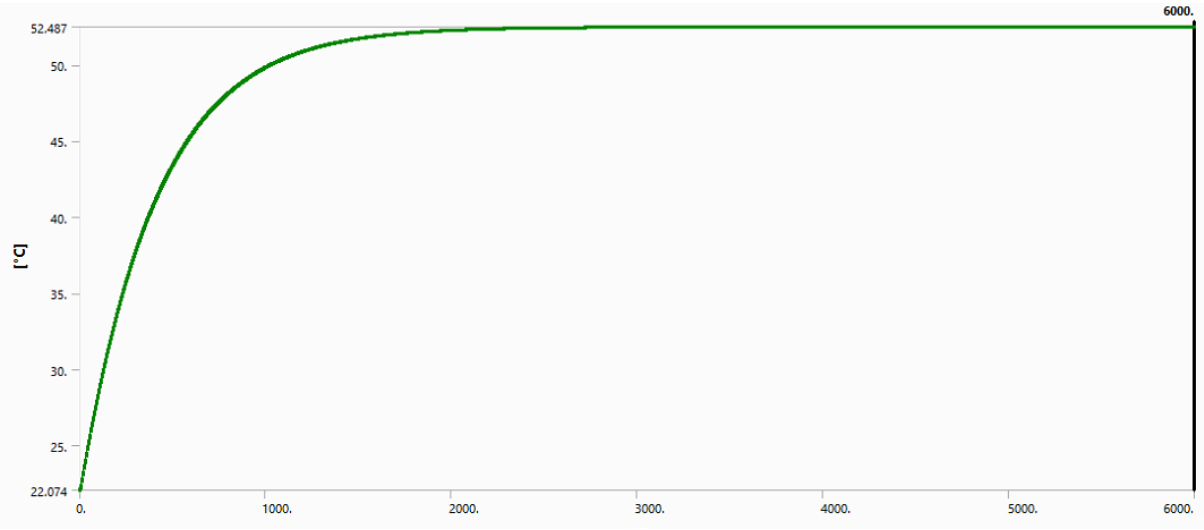

Figure 3.21 The Validating Result of 3-D Simulation with 23W Load

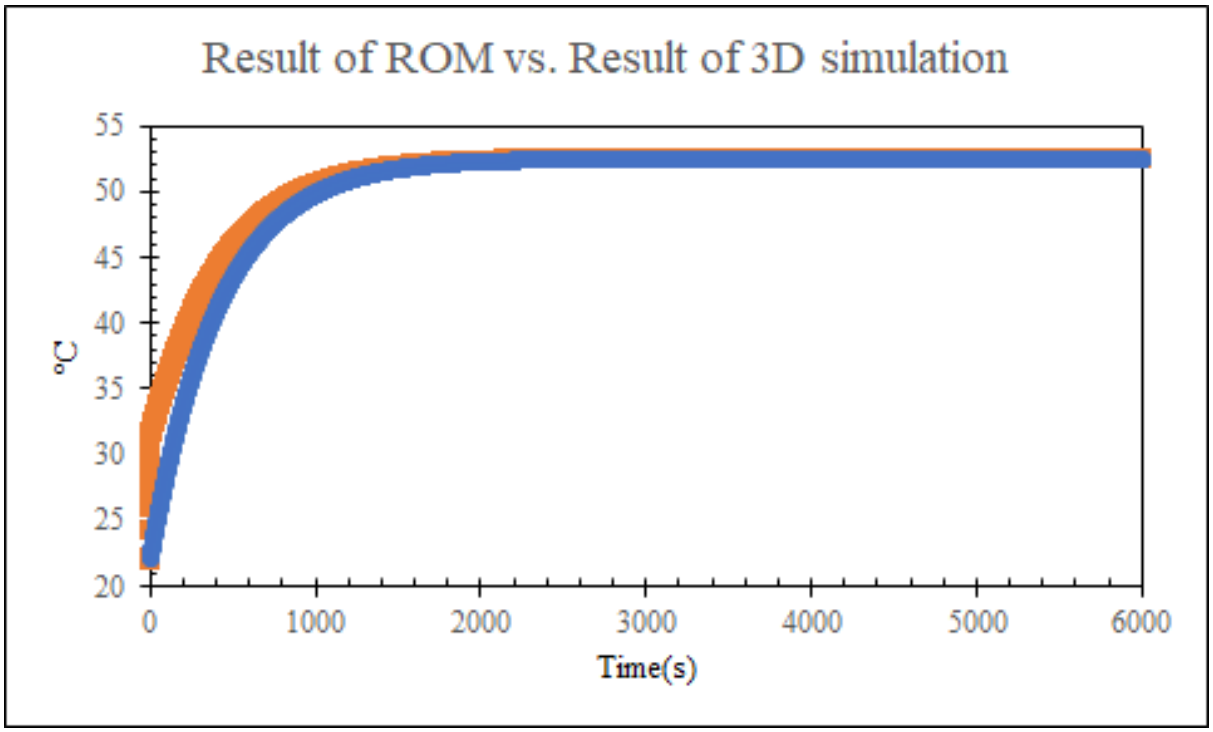

Figure 3.22 Result of ROM vs. Result of 3-D Simulation

3.4 Experimental Results

To get a full picture of the temperature distribution across the motor's surface while operating at its utmost acceleration of 9 m/s², we strategically positioned five LM35 temperature sensors uniformly along the top surface of the motor. This meticulous arrangement allowed us to capture a detailed snapshot of temperature variations.

The temperature monitoring results, depicted in Figure 3.23., provide a visual representation of the intricate temperature distribution observed across the motor's surface during its operation under the highest acceleration conditions. These observations form a critical component of our investigative pursuit, providing invaluable insights into the thermal dynamics and behavior of the linear magnetic system.

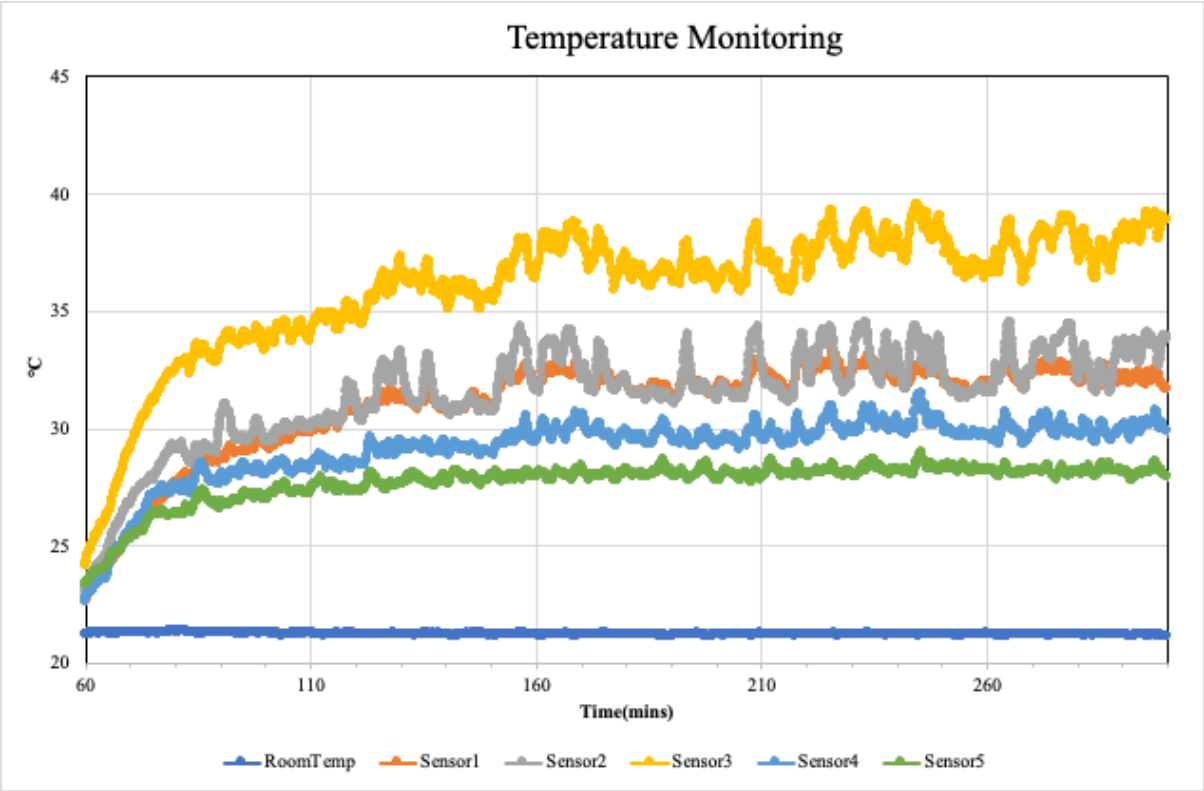

Figure 3.23 Temperature Monitoring at the Surface of the Motor

4. Summary of Results

We have presented the results of our multi-order modeling approach, encompassing a mesh convergence test, 3-D simulations, reduced-order modeling validation, and experimental findings. Now, let's delve further and establish the connections that bind these diverse outcomes into a coherent understanding.

4.1 Mesh Convergence Test

In the context of the mesh convergence test, the difference in maximum temperatures amounts to less than two percent. This discrepancy falls within an acceptable and appropriate range, rendering the utilization of a ten-millimeter length mesh suitable. In essence, a larger side length for the mesh element corresponds to a reduced requirement for the number of elements in the model.

However, a closer examination of Figure 4.3 and Figure 4.4 highlights a noteworthy phenomenon: both the 7.5-mm and 10-mm models exhibit undershooting in their minimum temperature values. This observation prompts a reconsideration of the mesh size's influence. Given the manifestation of undershooting, a prudent course of action involves diminishing the mesh size to enhance precision. Consequently, we arrived at the decision to adopt a 5-mm mesh element size for our simulations. This choice, underpinned by the objective of mitigating undershooting and elevating precision, ensures a more robust and accurate modeling approach.

4.2 Transient 3-D Simulation and Thermal Experiment

Numerical simulation serves as a high-fidelity technique for scrutinizing intricate models. In our specific context, we harnessed the ANSYS Transient Thermal module to comprehensively examine the thermal dynamics within the linear magnetic driving system. Drawing insights from our experimental endeavors, it becomes evident that when the motor operates at its peak acceleration in the absence of payloads, the power consumption gravitates around the 20W mark. The outcomes stemming from both the experiment and the simulation are concisely portrayed in Figure 4.1and Figure 4.2, respectively. These visual depictions encapsulate the convergence between empirical findings and simulation results, bolstering our understanding of the thermal behavior of the linear magnetic driving system.

Indeed, a parallel examination of the thermal behavior reveals striking similarities between the experiment and the simulation. Both models exhibit a convergence towards a quasi-static state over a duration of approximately 1,200 seconds. However, disparities in temperature readings can be attributed to the following factors:

- **Unstable Convection in the Experiment:** The experiment encountered challenges in maintaining stable convection, which could have contributed to temperature variations. Fluctuations in convection affect the heat transfer dynamics and subsequently influence temperature measurements.
- **Airflow Generated by the Moving Part (Puck):** The movement of the puck generates airflow within the experimental setup. This airflow has the effect of reducing the measured temperature, as it contributes to enhanced heat dissipation from the surface. Consequently, the experimentally measured temperature is anticipated to be lower than the simulated value.

In essence, while temperature disparities exist, the underlying thermal behavior remains consistent between the two models. The experiment's lower measured temperature, influenced by factors like unstable convection and the airflow generated by the moving part, aligns with the simulation's thermal trends. This convergence in thermal behavior underscores the effectiveness of our modeling approach in capturing the real-world dynamics of the linear magnetic driving system.

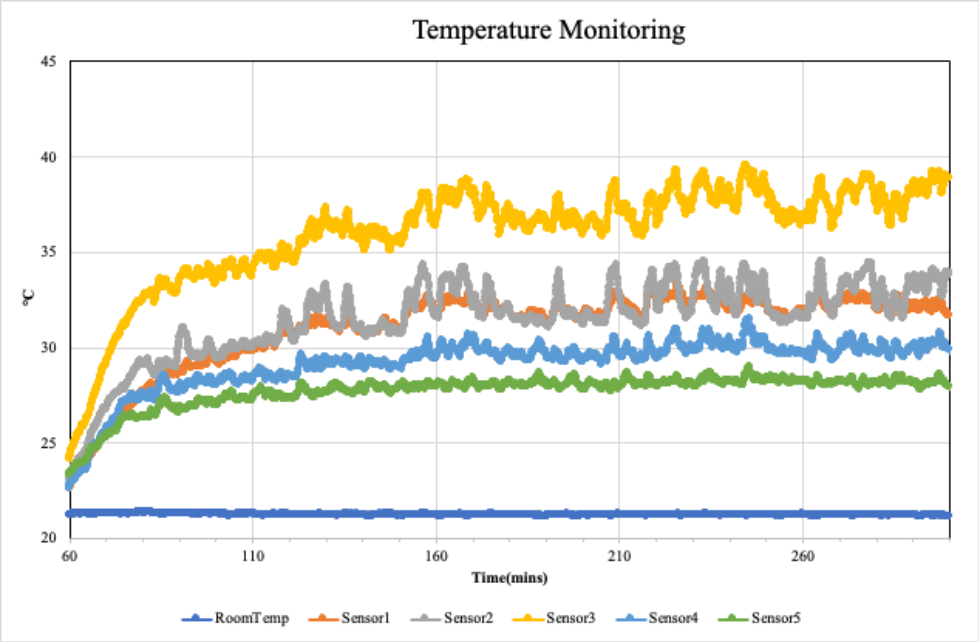

Figure 4.1 Temperature Monitoring at the Surface of the Motor

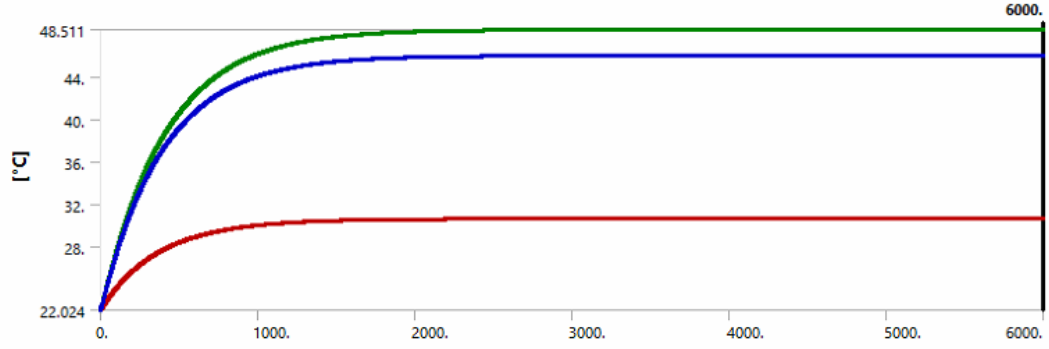

Figure 4.2 Transient Thermal Simulation Result with 20W Load

4.3 Reduced-order model building and validating

Leveraging the simulation results as learning scenarios, we proceeded to formulate and validate the reduced-order model (ROM). The outcomes, showcased in Figure 4.18 and 4.19, distinctly illustrate the alignment between the simulation and ROM results, with an impressively low error margin of below 0.1%. This robust agreement serves to validate the efficacy and accuracy of our ROM approach.

To further expand the scope, we introduced a new scenario in the realm of 3-D simulations. In this scenario, we introduced a 23W load as an input, aiming to assess the ROM's predictive capabilities under altered conditions. Impressively, as depicted in Figure 4.18 to Figure 4.22, the ROM results consistently demonstrate a high degree of accuracy, effectively mirroring the 3-D simulation outcomes within a matter of seconds. This swift and acceptable alignment attests to the ROM's proficiency in delivering reliable predictions even in scenarios beyond its training scope.

4.4 Comparing Time: Full 3-D vs. Dynamic ROM Simulations

Concluding our discussion on the experiment, 3-D numerical simulation, and ROM simulation results, let us shift our focus to the critical aspect of simulation runtimes. It is universally acknowledged that incorporating a greater number of elements in a physical model enhances the accuracy of the results. However, this augmentation in accuracy comes at a cost – the computational time. In this pursuit, CAE engineers are tasked with striking a delicate balance between precision and the expenditure of computational resources. Moreover, they must judiciously allocate priorities for running simulations.

To illuminate this concept further, we present Table 4-1 and Figure 4.3, both of which provide a comprehensive overview of the time consumption associated with both 3-D simulations and ROM simulations. These representations underline the intricate interplay between accuracy and computational efficiency, offering a tangible illustration of the trade-off that CAE engineers strategically navigate to achieve optimal results within pragmatic timeframes.

Table 4-1 Time Consumption of for 6,000 sec transient simulation

	10mm	7.5mm	5mm	2.5mm	ROM
Time Consumption(s)	668	1047	1,232	6,720	9

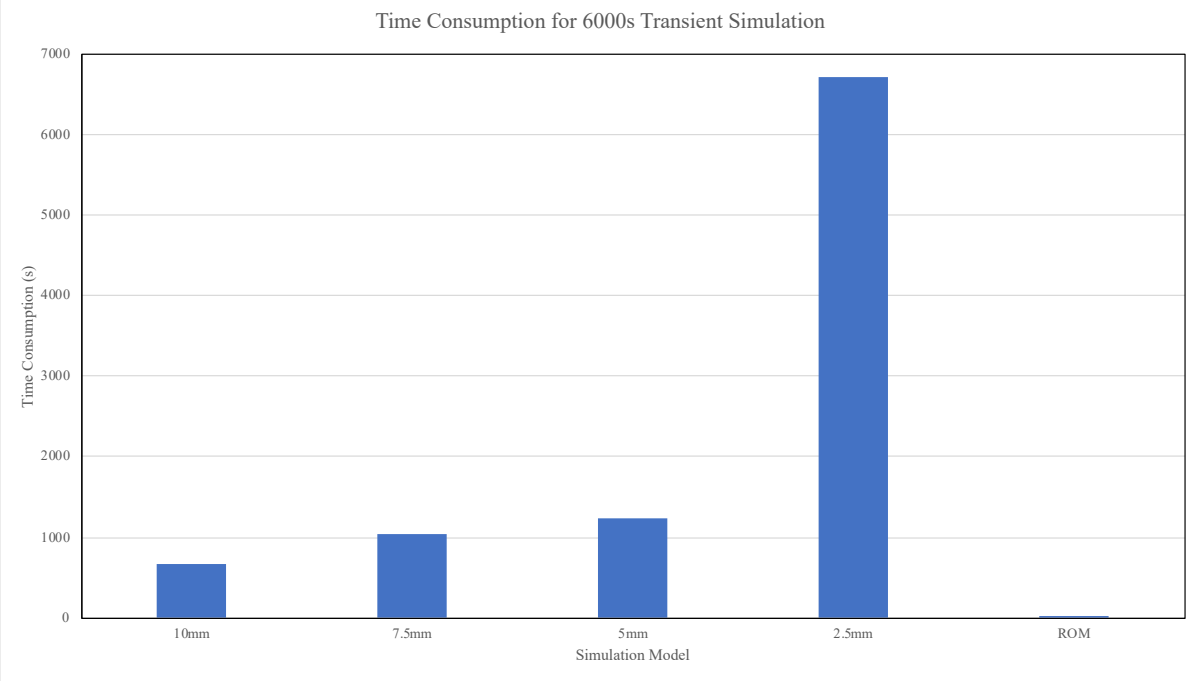

Figure 4.3 Time Consumption for 6,000 sec Transient Simulation

The difference in time between 3-D simulation and ROM simulation is substantial. Opting for quasi-real-time results comes with a trade-off: an error under 0.1%. Yet, this compromise yields a significant benefit. The reduced-order model becomes a valuable tool,

enabling developers and CAE engineers to swiftly test ideas and assumptions. This efficiency accelerates innovation, offering a nimble approach to tackle complex challenges with confidence. In essence, the reduced-order model strikes a balance between precision and speed, enhancing simulations' effectiveness.

5. Future Work

Reflecting on the motivations behind constructing finite element models, the overarching objective is clear: to empower engineers in curtailing time and costs associated with trial and error. It is not uncommon for simulations to require days for completion. Enter Reduced-Order Modeling (ROM), a tool tailor-made for developers, streamlining their ideation process. This acceleration in the development timeline holds the potential to expedite the advent of new technologies.

Let's illustrate this with a tangible case. While a 3-D transient thermal simulation for a motor may demand approximately half an hour, the ROM accomplishes the same task within mere seconds. This astonishing swiftness in predicting model behavior propels the realization of the digital twin concept. The digital twin leverages real-time simulation data as virtual sensors, facilitating the monitoring of operational conditions in demand systems. Through this innovation, engineers can mitigate unforeseen downtime, thereby enhancing system reliability.

Our next endeavor involves the application of this concept in constructing the digital twin—a significant stride towards fostering a harmonious synergy between virtual simulation and real-world operations.

References

[1] Wan, Y.-T. (2006). MATERIAL TRANSPORT SYSTEM DESIGN IN MANUFACTURING. Georgia Institute of Technology.

[2] Palka, R., & Woronowicz, K. (2021). Linear Induction Motors in Transportation Systems. Energies, 14(9), 2549.

[3] Linear Motors Application Guide. (n.d.). Aerotech, Inc.

[4] MagneMotion MagneMover LITE User Manual. (n.d.). MagneMotion, Inc.

[5] COLLINS, D. (2021, March 31). The benefits—And drawbacks—Of linear motors for dynamic applications. LINEAR MOTION TiPS.

[6] Song, Y., Darani, K. S., Khdair, A. I., Abu-Rumman, G., & Kalbasi, R. (2021). A review on conventional passive cooling methods applicable to arid and warm climates considering economic cost and efficiency analysis in resource-based cities. Energy Reports, 7, 2784–2820.

[7] Sabbah, R., Kizilel, R., Selman, J. R., & Al-Hallaj, S. (2008). Active (air-cooled) vs. passive (phase change material) thermal management of high power lithium-ion packs: Limitation of temperature rise and uniformity of temperature distribution. Journal of Power Sources, 182(2), 630–638.

[8] Lumley, J.L. (1967) The Structure of Inhomogeneous Turbulent Flows. In: Yaglom, A.M. and Tartarsky, V.I., Eds., Atmospheric Turbulence and Radio Wave Propagation, 166-177.

[9] Far, M. F., Mukherjee, V., Martin, F., Rasilo, P., & Belahcen, A. (2018). Model Order Reduction of Bearingless Reluctance Motor Including Eccentricity. 2018 XIII International Conference on Electrical Machines (ICEM), 2243–2249.

[10] Boscaglia, L., Boglietti, A., Nategh, S., Bonsanto, F., & Scema, C. (2021). Numerically Based Reduced-Order Thermal Modeling of Traction Motors. IEEE Transactions on Industry Applications, 57(4), 4118–4129.

[11] Cui, F., Sun, Z., Xu, W., Qian, H., & Cao, C. (2021). Optimization Analysis of Long Primary Permanent Magnet Linear Synchronous Motor. IEEE Transactions on Applied Superconductivity, 31(8), 1–4.

[12] Abbadi, M. (2004). Modeling and Control of a Magnetic Levitation System. Department of Electrical and Computer Engineering-Bradley University.

[13] Ozeki, M. (1997). Development of the Superconducting Maglev System in Japan. In Proceedings of the Sixteenth International Cryogenic Engineering Conference/International Cryogenic Materials Conference (pp. 13–18). Elsevier.

[14] Yi, C., Hofmann, H., & Epureanu, B. I. (2021). Reduced-order models for electro-magnetic-structural coupling phenomena. Mechanical Systems and Signal Processing, 159, 107752.

[15] Chaban, A., Lukasik, Z., Lis, M., & Szafraniec, A. (2020). Mathematical Modeling of Transient Processes in Magnetic Suspension of Maglev Trains. Energies, 13(24), 6642.

[16] Saha, S., & Nabi, M. (2019). Control of Axial Active Magnetic Bearing using Reduced Order Model. 2019 8th International Conference on Modeling Simulation and Applied Optimization (ICMSAO), 1–5.

[17] Yi, C., Hofmann, H., & Epureanu, B. I. (2021). Reduced-order models for electro-magnetic-structural coupling phenomena. Mechanical Systems and Signal Processing, 159, 107752.

[18] Sancarlos, A., Cueto, E., Chinesta, F., & Duval, J.-L. (2021). A novel sparse reduced order formulation for modeling electromagnetic forces in electric motors. SN Applied Sciences, 3(3), 355.

[19] Dai, J., Xia, J., Wang, C., & Xu, S. (2017). Thermal analysis of an electromagnetic linear actuator. Advances in Mechanical Engineering, 9(12), 168781401774538.

[20] Ruiz-Rojas, E. D., Vazquez-Gonzalez, J. L., Alejos-Palomares, R., Escudero-Uribe, A. Z., & Mendoza-Vázquez, J. R. (2008). Mathematical Model of a Linear Electric Actuator

with Prosthesis Applications. 18th International Conference on Electronics, Communications and Computers (Conielecomp 2008), 182–186.

[21] MagneMotion MagneMover LITE User Manual. (n.d.). MagneMotion, Inc.

[22] Sarwar, A., Nemirovski, A., & Shapiro, B. (2012). Optimal Halbach Permanent Magnet Designs for Maximally Pulling and Pushing Nanoparticles. Journal of Magnetism and Magnetic Materials, 324(5), 742–754.

[23] Hor, P. J., Zhu, Z. Q., Howe, D., & Rees-Jones, J. (1998). Minimization of cogging force in a linear permanent magnet motor. IEEE Transactions on Magnetics, 34(5), 3544–3547.

[24] Zhu, Z. Q., Hor, P. J., Howe, D., & Rees-Jones, J. (1997). Calculation of cogging force in a novel slotted linear tubular brushless permanent magnet motor. IEEE Transactions on Magnetics, 33(5), 4098–4100.

[25] Dhondt, G. (n.d.). CalculiX CrunchiX USER'S MANUAL version 2.7. https://web.mit.edu/calculix_v2.7/CalculiX/ccx_2.7/doc/ccx/ccx.html

[26] MagneMover LITE User Manual. (n.d.). MagneMotion, Inc. https://literature.rockwellautomation.com/idc/groups/literature/documents/um/mmi-um002_-en-p.pdf

[27] LM35 Precision Centigrade Temperature Sensors. (n.d.). TEXAS INSTRUMENTS. https://www.ti.com/lit/ds/symlink/lm35.pdf

[28] viastore SYSTEMS. (n.d.). MINIMIZE YOUR THROUGHPUT AND DELIVERY TIMES!

[29] Siegel, R., & Howell, J. (n.d.). THERMAL RADIATION HEAT TRANSFER.

[30] Twin Builder Help. (2021). ANSYS, Inc.

[31] LeCun, Y., Bengio, Y., & Hinton, G. (2015). Deep learning. *Nature*, *521*(7553), 436–444.

[32] Kosky, P., Balmer, R., Keat, W., & Wise, G. (2013). Mechanical Engineering. In Exploring Engineering (pp. 259–281). Elsevier. https://doi.org/10.1016/B978-0-12-415891-7.00012-1